Journal of Dermatological Science (2008) 51, 113—120

ELSEVIER

Journal of Dermatological SCIENCE

www.intl.elsevierhealth.com/journals/jods

Sequence analysis of filaggrin gene by novel shotgun method in Japanese atopic dermatitis

Takashi Sasaki [a,b], Jun Kudoh [a,b], Tamotsu Ebihara [c], Aiko Shiohama [a,b], Shuichi Asakawa [a], Atsushi Shimizu [a], Atsushi Takayanagi [a], Itaru Dekio [c], Chieko Sadahira [c], Masayuki Amagai [c], Nobuyoshi Shimizu [b,*]

[a] *Department of Molecular Biology, Keio University School of Medicine, 35 Shinanomachi, Shinjuku-ku, Tokyo 160-8582, Japan*
[b] *Advanced Research Center for Genome Super Power, Keio University, 2 Okubo, Tsukuba, Ibaraki 300-2611, Japan*
[c] *Department of Dermatology, Keio University School of Medicine, 35 Shinanomachi, Shinjuku-ku, Tokyo 160-8582, Japan*

Received 27 October 2007; received in revised form 4 February 2008; accepted 21 February 2008

KEYWORDS
Filaggrin;
Atopic dermatitis;
DNA sequencing;
Shotgun

Summary

Background: Recent reports indicated that nonsense mutations in filaggrin (FLG) found in ichthyosis vulgaris (IV) patients are predisposing factors for atopic dermatitis (AD) with asthma. The exon 3 of FLG contains tandemly repeated, highly homologous, 11—13 sequence units of 972 or 975 bp, each of which corresponds to the coding sequence of the processed filaggrin with slight sequence difference. This unique gene structure has hampered the precise DNA sequence determination.
Objective: We developed a novel DNA sequencing method "FLG-shotgun" to directly characterize the mutations in Japanese AD patients.
Methods: We examined 24 Japanese AD patients with "FLG-shotgun" method.
Results: Multiple units of FLG were amplified by PCR using several sets of common primers for the conserved regions, and DNA sequences of each cloned PCR product were determined. Multiple reads of DNA sequences in both alleles were aligned and re-constructed to cover the entire coding regions. We found three major genotypes (A, B, and C) which represent different numbers (11—13) of homologous sequence units. Furthermore, we found two novel nonsense mutations; one mutation 8666-8667CC>GA on the unit 9 of allele B that causes a nonsense mutation S2899X in two patients and the other mutation 9887C>A on the unit 10 of allele B that causes a nonsense mutation S3296X in two patients.

* Corresponding author. Tel.: +81 29 865 1641; fax: +81 29 865 1641.
E-mail address: smzgsp@dmb.med.keio.ac.jp (N. Shimizu).

doi:10.1016/j.jdermsci.2008.02.009

Conclusion: We found two novel FLG mutations by directly analyzing Japanese patients with AD. FLG-shotgun will provide a valuable tool to further define the nature of the AD phenotype associated with FLG mutations.

1. Introduction

Filaggrin (FLG) is a major epidermal protein and expressed as a profilaggrin of >500 kDa in the prominent keratohyalin granules of outer epidermis [1,2]. The profilaggrin is processed by protease to filaggrin of 35 kDa and the resulting filaggrins are cross-linked by transglutaminase to build skin barrier [3]. The skin barrier is indispensable to prevent invasion of micro-organisms, chemical compounds and allergens, and to keep moisture level of the skin [2], therefore, the reduced filaggrin production would disturb skin barrier formation.

Ichthyosis vulgaris (IV; OMIM no. 146700) is one of the most common genetic skin disorder [4]. The clinical features of IV include palmar hyperlinearity, keratosis pilaris and scaling at lower abdomen, arms and legs [5]. Thirteen kinds of FLG gene mutations were found in the IV and atopic dermatitis (AD) patients from European population [6–8], and two different kinds of mutations (S2554X and 3321delA) were found in the Japanese IV patients ([9], Nomura et al.). These results indicated that FLG gene mutations produce reduced amounts of filaggrin protein which would generate IV phenotypes.

AD frequently coincides with keratosis pilaris, allergy, and asthma, and AD patients have increased recently in the developed world. Importantly, AD and keratosis pilaris are commonly found in IV. Actually, recent reports indicated that nonsense mutations in FLG gene found in IV patients are predisposing factors for AD with asthma [6–13]. These results strongly suggest that predisposing factors for AD include not only immune-deficiency but also skin barrier deficiency.

The FLG is located on human chromosome 1q21.3 as a member of the large gene cluster "epidermal differentiation complex (EDC)" involved in the terminal differentiation. The EDC gene cluster is composed of FLG, six FLG-related genes, and genes for S100 family, small proline-rich protein family, loricrin, involcrin and so on [14]. The FLG gene consists of three exons and produces a transcript of 12,747 nt [15,16]. Interestingly, relatively large exon 3 (12,048 bp) contains all the coding sequence to encode a large profilaggrin of >500 kDa and in fact it consists of 11 homologous sequence units of 972 or 975 bp, each of which corresponds to the coding sequence of the processed filaggrin with slight sequence difference. Hence, precise DNA sequence determination has been hampered by these multiple units of homologous sequence.

In this study, we developed a shotgun DNA sequencing method "FLG-shotgun" specialized for FLG. As a result of FLG-shotgun of 24 Japanese AD patients, we isolated three major genotypes (A–C) containing 11, 13, and 12 FLG homologous sequence units, respectively. Furthermore, we found two novel nonsense mutations on type B allele. These results indicated efficiency of FLG-shotgun for DNA sequence of FLG in AD patients.

2. Materials and methods

2.1. Clinical materials

Blood samples were obtained from 24 Japanese AD patients, who have been suffering from severe, itchy, chronically relapsing, inflammatory skin condition for a long time, and observation of total IgE amount incensement. The diagnosis of atopic dermatitis was made using the AD diagnostic criteria by Japanese Dermatological Association. Among these 24 Japanese AD patients, there is no IV patient who shows palmar hyperlinearity and typical scaling at arms and legs. This study was approved by the committee for medical ethics at Keio University.

2.2. FLG-shotgun

Genomic DNA was isolated from peripheral bloods or saliva by PAX gene Blood DNA kit (Qiagen). The homologous sequence region in FLG was amplified by Expand High Fidelity PCR polymerase (Roche) with four distinct primer sets: FLG set1 FLGREP-24F and mixture of FLGREP-965R1/R2/R3, FLG set2 FLGREP-487F and FLGREP-463R, FLG set3 FLGREP-257F and FLGREP-215R, FLG set4 FLGREP-683F and FLGREP-669R (see Supplementary Table 1 for primer DNA sequence). Thus, segments of 900–950 bp can be amplified with small overlaps. PCR amplification condition was as follows, 1 cycle of 94 8C for 2 min,

35 cycles of 94 8C for 30 s, 60 8C for 1 min, and 72 8C for 4 min, and 1 cycle of 72 8C for 5 min. The PCR products were purified with Wizard plus SV minipreps DNA purification system (Promega) and ligated into TA cloning vector pGEM-tEasy (Promega). *E. coli* was transformed with these DNAs and isolated colonies were inoculated into 384-well plates. The plasmid DNA in the *E. coli* of each well was amplified by TempliPhi DNA Amplification kit (GE healthcare bioscience), and was sequenced by each primer for PCR reaction using Big Dye ver. 3.1 and 3730 DNA analyzer (Applied Biosystems). Phred/Phrap/Consed was used for assembly of DNA sequences.

Exon 2 was amplified by PCR with FLGexon2F and FLGexon2R. Both terminal regions in exon 3 (Fig. 2) were amplified by PCR with FilLR2F and FLGREP-215R, and FLGREP-487F and FilLR1R. These PCR products were sequenced as described above.

2.3. Long PCR of whole homologous sequence region in FLG

Whole homologous sequence region in FLG was amplified by Long PCR as described previously with slight modification, namely, KOD FX (TOYOBO) was used as DNA polymerase [6].

3. Results

3.1. FLG-shotgun DNA sequencing

The FLG consists of three exons and relatively large exon 3 (12,048 bp) contains all the coding sequence to encode a large profilaggrin of >500 kDa and in detail it consists of 11 homologous sequence units (Fig. 1A and B). These homologous sequence units correspond to the coding sequence of each of the processed filaggrins with slight sequence difference. In fact, the self dot matrix analysis of FLG cDNA sequence (Ref seq ID: NM_002016) revealed 11 homologous sequence units within a region (892–11,773 nt) and a small sequence of 184 bp after 11th unit (Fig. 1B and C). Those homologous sequence units are extremely similar to each other, and their length is commonly 972 bp except that units 2 and 6 are 3 bp larger than others (Fig. 1D). Therefore, it was hard to precisely analyze each homologous sequence unit with high accuracy.

To solve this problem, we applied the shotgun DNA sequencing method to genomic DNA for 20-kbp FLG and developed a "FLG-shotgun" method (Fig. 2). The first step of FLG-shotgun involves PCR-amplification of all homologous sequence units using

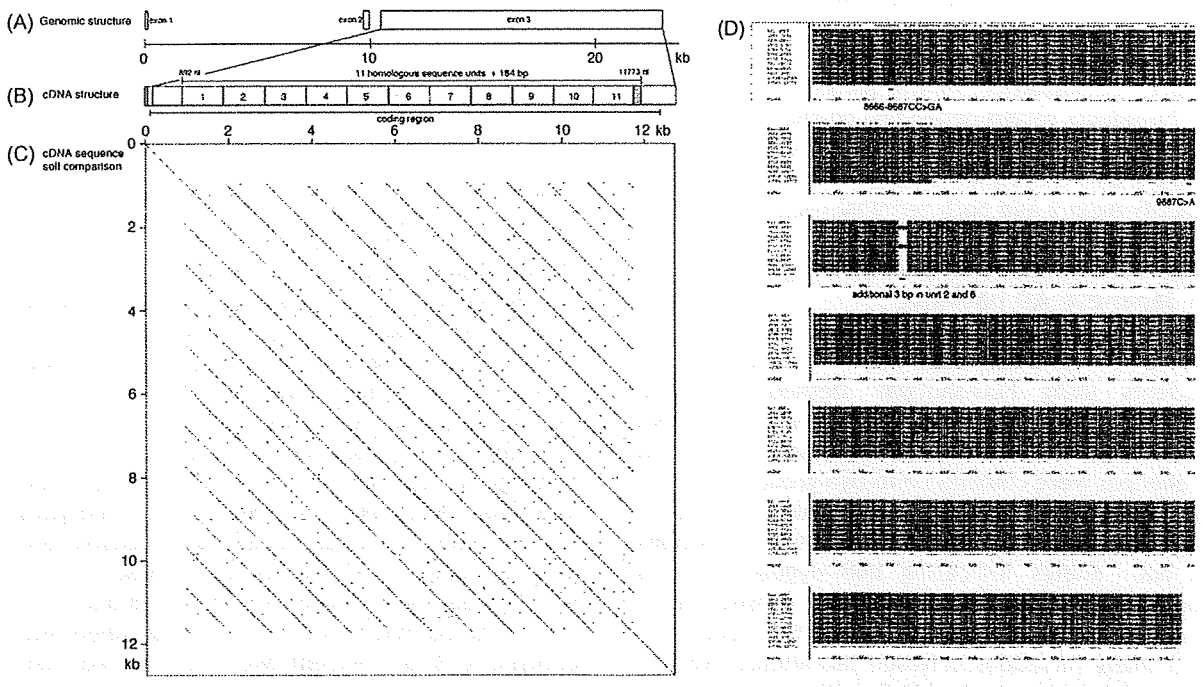

Fig. 1 Features of human filaggrin (FLG) gene. (A) Genomic structure. The FLG gene consists of three exons. (B) cDNA structure (NM_002016). Exon 3 is composed of eleven homologous sequence units of 972 or 975 bp each of which encodes filaggrin. These units are located in tandem at a region 892–11,773 nt. (C) The self dot matrix analysis of FLG cDNA sequence (NM_002016). This figure indicates eleven homologous sequence units of 972 or 975 bp and one small unit of 184 bp. (D) The DNA sequence alignment of FLG cDNA (NM_002016). Three-base insertion and two novel nonsense mutations can be seen.

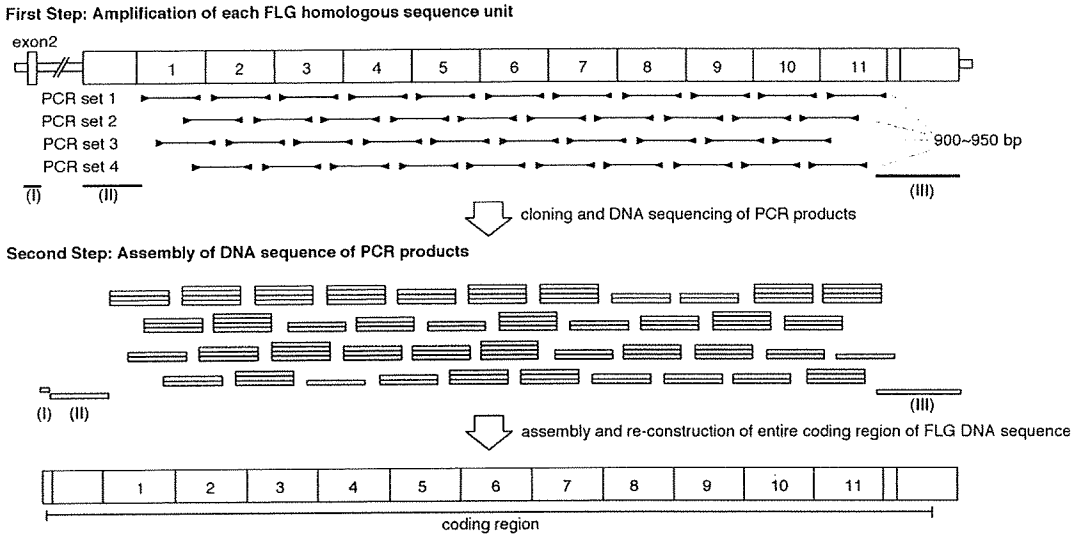

Fig. 2 Strategy of FLG-shotgun DNA sequencing and data assembly. First step involves the PCR-amplification of each homologous sequence unit using four sets of primers which amplify every 900–950 bp. Also, primer sets for exon 2 (I), the distal (II) region of unit 1, and proximal (III) region of unit 11 are indicated as thick lines. Second step involves the assembly of DNA sequences to assemble each unit and finally re-construct entire ORF region of FLG DNA sequence. The amount of PCR products varies depending on the genotypes.

four different sets of PCR primers that cover 900–950-bp segments with slight overlaps. The PCR products were cloned into plasmids and individually sequenced. The second step involves assembly of DNA sequences to determine each homologous sequence units and eventually re-construct the entire FLG sequence. At this stage, the amount of PCR products varied depending on the patient genotypes as illustrated in Fig. 2. Furthermore, three additional PCR-primer sets (I–III) were used to amplify exon 2 and both terminal region of exon 3.

3.2. Identification of three FLG genotypes in Japanese AD patients

We determined FLG sequence of 24 Japanese AD patients using FLG-shotgun method described above. At the first step of assembly of DNA sequence, we noticed that assembled FLG sequences were classified into two groups. The first group consists of nine cases and has almost identical sequence with no or a few heterozygous nucleotides in both alleles indicating homozygote for FLG sequence, while the second group consists of 15 cases has apparently heterozygous FLG sequences with many variations between two alleles. We first determined homozygous FLG sequences and they were classified into three major genotypes (A–C) as described below.

Homozygous genotype A was found in 3 AD patients (P006, P008, and P011) and was matched with reference sequence of FLG cDNA sequence (NM_002016) containing 11 homologous sequence units except a few SNPs. Fig. 3A shows a representative DNA sequencing data for the patient P008. In this case, we could re-construct the continuous entire FLG sequence with only two heterozygous nucleotides.

Homozygous genotype B consists of 13 homologous sequence units and was found in 4 Japanese AD patients (P005, P007, P017, and P023). We precisely determined FLG sequence of genotype B with four primer sets, and a representative DNA sequencing data for the patient P023 was shown in Fig. 3B.

Homozygous genotype C consists of 12 homologous sequence units and was found in 2 Japanese AD patients (P001 and P022). We precisely determined FLG sequence of genotype C with four primer sets (Fig. 3C). In both these cases, only a single continuous FLG sequence was assembled.

In other 15 AD patients, we assembled over 20 homologous sequence units first. It apparently indicated that they have two different FLG genotypes on distinct alleles. In these cases, we re-constructed two FLG sequences on distinct alleles based on the SNPs between two alleles. As a result, 28 out of 30 re-constructed FLG sequences were classified into genotype A, B, or C except two cases derived from one allele of P019 and P021 (Table 1). Although FLG sequences of these two alleles were basically matched with genotype B FLG, two homologous sequence units were lost, resulting in 11 homologous sequence units (Fig. 4A). We designated this genotype as type Bs.

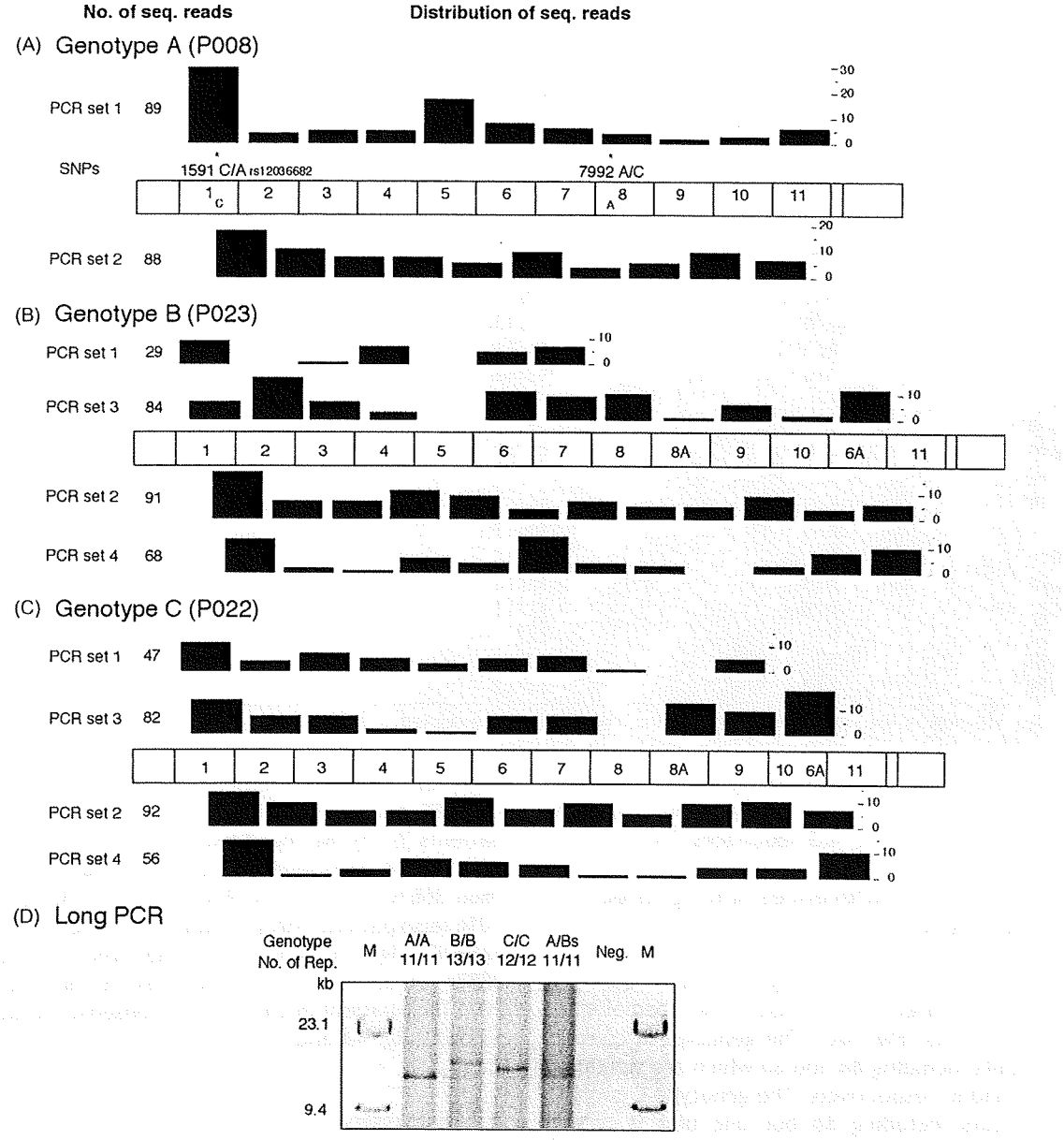

Fig. 3 Schematic representation of data analysis for genotypes A, B, and C of FLG. The frequency of sequence-reads is indicated by thickness of black rectangles. (A) The genotype A of FLG. The FLG DNA sequence of genotype A was re-constructed by two sets of PCR (set 1 and set 2). Two heterozygous nucleotides (1591 C/A and 7992 A/C) were found in genotype A of FLG derived from P008. (B) The genotype B of FLG. The FLG DNA sequence of genotype B was re-constructed by four sets of PCR (sets 1–set 4). No heterozygous nucleotides was found in genotype B of FLG derived from P023. (C) The genotype C of FLG. The FLG DNA sequence of genotype C was re-constructed by four sets of PCR (set 1–set 4). No heterozygous nucleotides was found in genotype C of FLG derived from P022. (D) Long PCR analysis of genotypes A–C, and Bs of FLG. P008 (A/A), P023 (B/B), P022 (C/C), and P021 (A/Bs) were used as representatives of each genotype.

Finally, we found three major (A–C) and one minor (Bs) genotypes for the FLG gene of 24 Japanese AD patients (Table 1). There are four cases (P001, P005, P022, and P023) for which no heterozygous nucleotide was detected perhaps because DNA sequence of two alleles are identical or one allele is deleted.

To confirm the reliability of these re-constructed FLG sequences, we compared the length of long PCR products which include whole homologous sequence units region (Fig. 3D). We found that the length of long PCR products observed are consistent with the number of homologous sequence units in reconstructed FLG sequences of each genotype. These

Table 1 Genotype and mutation analyses of FLG for 24 Japanese AD patients

Patients	FLG genotype	No. of units per allele	Nonsense mutation
P001	C[a]	12[a]	–
P002	A/B	11/13	–
P003	A/B	11/13	–
P004	A/B	11/13	–
P005	B[a]	13[a]	–
P006	A/A	11/11	–
P007	B/B	13/13	–
P008	A/A	11/11	–
P009	B/C	13/12	–
P010	A/B	11/13	–
P011	A/A	11/11	–
P012	B/C	13/12	–
P013	A/C	11/12	–
P014	A/B	11/13	–
P015	A/C	11/12	–
P016	A/B	11/13	8666-8667CC>GA (B)
P017	B/B	13/13	–
P018	A/B	11/13	–
P019	A/Bs	11/11	9887C>A (Bs)
P020	A/B	11/13	8666-8667CC>GA (B)
P021	A/Bs	11/11	9887C>A (Bs)
P022	C[a]	12[a]	–
P023	B[a]	13[a]	–
P024	A/B	11/13	–

[a] DNA sequence of two FLG alleles are identical or one allele may be deleted.

results indicated that previously reported length polymorphism of FLG were derived from unit number difference among FLG sequences [3].

3.3. Sequence differences among three FLG genotypes

We identified three distinct genotypes (A–C) which represent different number of homologous sequence units (Fig. 4A). The genotype B consists of 13 units including 8A and 6A which are similar to units 8 and 6, respectively, The genotype C consists of 12 units including 8A but one unit is lacked between unit 10 and unit 6A comparing with genotype B. The genotype Bs lacked unit 8A and 9 from genotype B, which would be subtypes of genotype B. Among these genotypes of FLG, we often identified single nucleotide sequence polymorphisms among these three genotypes (Supplementary Table 2). These sequence polymorphisms were valuable to precisely assemble each homologous sequence units, especially when patient's genotypes are heterozygous.

3.4. Two novel nonsense mutations in the FLG of Japanese AD patients

The previous reports showed thirteen different mutations in the FLG for European IV and AD patients, and two additional nonsense mutations (S2554X and 3323delA) for Japanese IV and AD patients [6–9]. We found two novel nonsense mutations in 24 Japanese AD patients: one mutation 8666-8667CC>GA on unit 9 of allele B in the patient P016 (also patient P020) causes a nonsense mutation S2899X (Fig. 4A and B) and the other mutation 9887C>A on unit 10 of allele Bs in the patient P021 (also patient P019) causes a nonsense mutation S3296X (Fig. 4A and C).

4. Discussion

In this study, we developed a shotgun DNA sequencing method "FLG-shotgun" specialized for determining DNA sequence of the complicated FLG that consists of 11–13 tandem homologous sequence units of 972 or 975 bp. In this method, multiple units of FLG homologous sequence are amplified by PCR using several sets of common primers which are designed at conserved region of multiple units, and DNA sequences of each PCR product were determined. Finally, DNA sequences of FLG in both alleles were re-constructed respectively using DNA sequence differences among each multiple units of homologous sequence. Previous studies used the several primer sets to amplify the specific region of these multiple units [8,9]. This method is one of

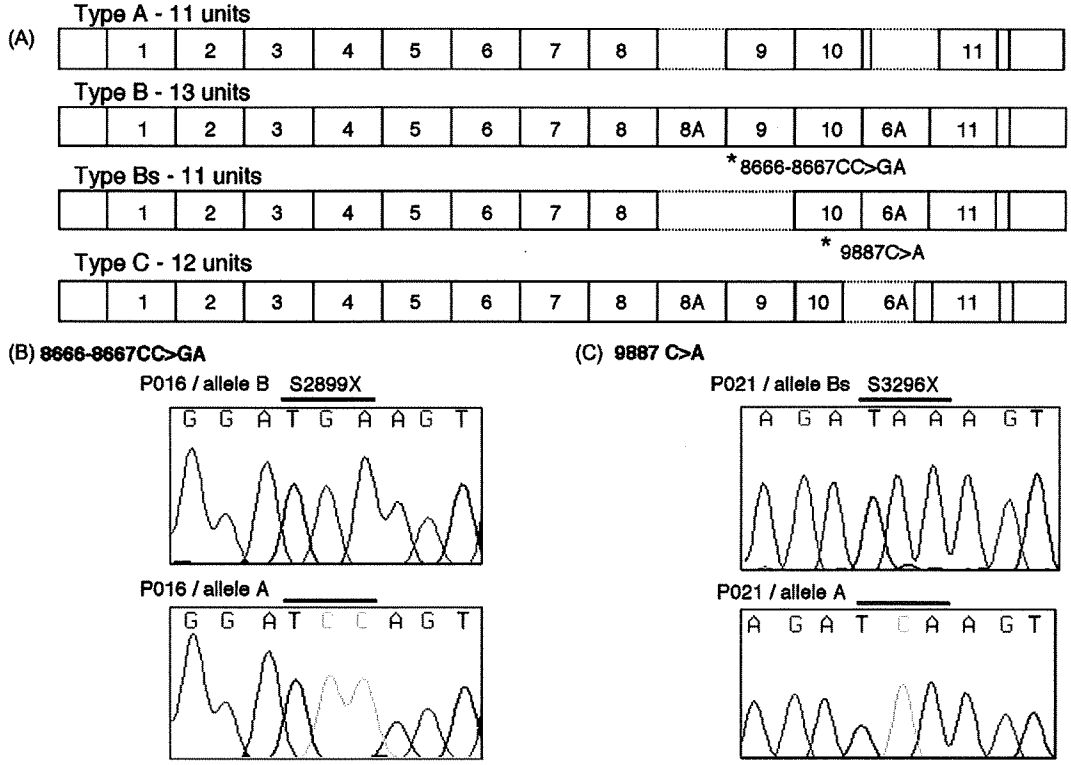

Fig. 4 The genotype of FLG and two novel nonsense mutations. (A) Three major (types A, B, and C) and one minor genotypes (type Bs) of FLG gene in Japanese AD patients. (B) The mutation 8666-8667CC>GA in the allele B of patient P016 as compared to the normal allele A. This mutation causes nonsense codon S2899X. (C) The 9887C>A mutation in the allele Bs of patient P021 as compared to the normal allele A. This mutation causes nonsense codon S3296X.

efficient method to determine the FLG DNA sequence, however, it is difficult to distinguish the DNA sequence of two alleles. Furthermore, there is a little possibility to miss the detection of the novel FLG genotype which is not amplified using current primer sets. Actually, number of these multiple units of homologous sequence is different in each individual [3,6]. Therefore, novel DNA sequencing method for FLG is worthwhile to know the detailed FLG DNA sequence information of each genotype.

As a result of FLG-shotgun of 24 Japanese AD patients, we identified three major genotypes (A–C) regarding difference in the number of homologous sequence unit. Previous report indicated that number of FLG homologous sequence unit varies from 10 to 12 [3]. We observed such variation but it ranged from 11 to 13 in Japanese AD patients, suggesting a significant difference in human races. This variation was also linked often with small nucleotide sequence differences within homologous sequence units.

We found two novel nonsense mutations (S2899X and S3296X) in Japanese AD patients. Previously, the most of nonsense mutations of FLG were identified from IV patients, and then were confirmed in AD patients. In this study, we directly found these two mutations in AD patients. Currently, there is no information whether all FLG mutations responsible for AD are common with IV. Further studies would be needed to confirm the association between IV and two novel FLG mutations that we found.

We could not find any other mutations that were reported for European and Japanese AD patients. Other study also reported no European type nonsense mutations in Japanese AD patients [6,9]. Therefore, the types of nonsense mutation would be different between European and Japanese populations. The nonsense mutations produce a truncated shorter profilaggrin which may still be processed to filaggrins. If this was the case, the reduced amounts of filaggrin would be insufficient to form strong skin barrier and in turn it would directly affect the patient phenotype. Further study will be necessary to confirm the relation between FLG gene mutations and production level of filaggrin in the AD patients. Moreover, in the EDC locus, there are six other FLG-related genes and these genes are possible to associate with the pathogenesis of AD. Therefore, the FLG-shotgun method would also be applicable to the association study of those genes in EDC to further elucidate the genetic basis of AD.

Acknowledgements

The authors thank to Dr. Kazunori Shibuya and Dr. Akiharu Kubo for useful discussion, and thank to M. Furuhashi, T. Adachi, and S.K. Ishikawa for their excellent technical assistance. This work was supported by a fund from Keio Medical Association, and by Health and Labour Sciences Research Grants for Research on Allergic Disease and Immunology from the Ministry of Health, Labour, and Welfare of Japan.

Appendix A. Supplementary data

Supplementary data associated with this article can be found, in the online version, at doi:10.1016/j.jdermsci.2008.02.009.

References

[1] Listwan P, Rothnagel JA. Keratin bundling proteins. Methods Cell Biol 2004;78:817–27.
[2] Candi E, Schmidt R, Melino G. The cornified envelope: a model of cell death in the skin. Nat Rev Mol Cell Biol 2005;6:328–40.
[3] Gan SQ, McBride OW, Idler WW, Markova N, Steinert PM. Organization, structure, and polymorphisms of the human profilaggrin gene. Biochemistry 1990;29:9432–40.
[4] Judge MR, McLean WHI, Munro CS. Disorders of keratinisation. Rook's textbook of dermatology, vol. 2. 2004. pp. 34.54–34.56.
[5] Sybert VP, Dale BA, Holbrook KA. Ichthyosis vulgaris: identification of a defect in synthesis of filaggrin correlated with an absence of keratohyaline granules. J Invest Dermatol 1985;84:191–4.
[6] Smith FJ, Irvine AD, Terron-Kwiatkowski A, Sandilands A, Campbell LE, Zhao Y, et al. Loss-of-function mutations in the gene encoding filaggrin cause ichthyosis vulgaris. Nat Genet 2006;38:337–42.
[7] Sandilands A, O'Regan GM, Liao H, Zhao Y, Terron-Kwiatkowski A, Watson RM, et al. Prevalent and rare mutations in the gene encoding filaggrin cause ichthyosis vulgaris and predispose individuals to atopic dermatitis. J Invest Dermatol 2006;126:1770–5.
[8] Sandilands A, Terron-Kwiatkowski A, Hull PR, O'Regan GM, Clayton TH, Watson RM, et al. Comprehensive analysis of the gene encoding filaggrin uncovers prevalent and rare mutations in ichthyosis vulgaris and atopic eczema. Nat Genet 2007;39:650–4.
[9] Nomura T, Sandilands A, Akiyama M, Liao H, Evans AT, Sakai K, et al. Unique mutations in the filaggrin gene in Japanese patients with ichthyosis vulgaris and atopic dermatitis. J Allergy Clin Immunol 2007;119:434–40.
[10] Palmer CN, Irvine AD, Terron-Kwiatkowski A, Zhao Y, Liao H, Lee SP, et al. Common loss-of-function variants of the epidermal barrier protein filaggrin are a major predisposing factor for atopic dermatitis. Nat Genet 2006;38:441–6.
[11] Marenholz I, Nickel R, Rüschendorf F, Schulz F, Esparza-Gordillo J, Kerscher T, et al. Filaggrin loss-of-function mutations predispose to phenotypes involved in the atopic march. J Allergy Clin Immunol 2006;118:866–71.
[12] Stemmler S, Parwez Q, Petrasch-Parwez E, Epplen JT, Hoffjan S. Two common loss-of-function mutations within the filaggrin gene predispose for early onset of atopic dermatitis. J Invest Dermatol 2007;127:722–4.
[13] Barker JN, Palmer CN, Zhao Y, Liao H, Hull PR, Lee SP, et al. Null mutations in the filaggrin gene (FLG) determine major susceptibility to early-onset atopic dermatitis that persists into adulthood. J Invest Dermatol 2007;127:564–7.
[14] Mischke D, Korge BP, Marenholz I, Volz A, Ziegler A. Genes encoding structural proteins of epidermal cornification and S100 calcium-binding proteins form a gene complex ("epidermal differentiation complex") on human chromosome 1q21. J Invest Dermatol 1996;106:989–92.
[15] Presland RB, Haydock PV, Fleckman P, Nirunsuksiri W, Dale BA. Characterization of the human epidermal profilaggrin gene. Genomic organization and identification of an S-100-like calcium binding domain at the amino terminus. J Biol Chem 1992;267:23772–81.
[16] Markova NG, Marekov N, Chipev CC, Gan SQ, Idler WW, Steinert PM. Profilaggrin is a major epidermal calcium-binding protein. Mol Cell Biol 1993;13:613–25.

nature genetics

A homozygous frameshift mutation in the mouse *Flg* gene facilitates enhanced percutaneous allergen priming

Padraic G Fallon[1], Takashi Sasaki[2,3], Aileen Sandilands[4], Linda E Campbell[4], Sean P Saunders[1], Niamh E Mangan[1], John J Callanan[5], Hiroshi Kawasaki[6], Aiko Shiohama[2,3], Akiharu Kubo[6], John P Sundberg[7], Richard B Presland[8,9], Philip Fleckman[9], Nobuyoshi Shimizu[3], Jun Kudoh[2,3], Alan D Irvine[1,10], Masayuki Amagai[6,11] & W H Irwin McLean[4,11]

Loss-of-function mutations in the *FLG* (filaggrin) gene cause the semidominant keratinizing disorder ichthyosis vulgaris[1] and convey major genetic risk for atopic dermatitis (eczema)[2–4], eczema-associated asthma[2,3] and other allergic phenotypes[5]. Several low-frequency *FLG* null alleles occur in Europeans and Asians, with a cumulative frequency of ~9% in Europe[4]. Here we report a 1-bp deletion mutation, 5303delA, analogous to common human *FLG* mutations, within the murine *Flg* gene in the spontaneous mouse mutant flaky tail (ft). We demonstrate that topical application of allergen to mice homozygous for this mutation results in cutaneous inflammatory infiltrates and enhanced cutaneous allergen priming with development of allergen-specific antibody responses. These data validate flaky tail as a useful model of filaggrin deficiency and provide experimental evidence for the hypothesis that antigen transfer through a defective epidermal barrier is a key mechanism underlying elevated IgE sensitization and initiation of cutaneous inflammation in humans with filaggrin-related atopic disease.

Eczema is a common disease affecting 15–30% of children and 2–10% of adults in developed countries[6]. There is a strong genetic association with atopic disorders including asthma, hay fever and food allergy[7]. Elevated total IgE is observed in 60–80% of individuals with eczema attending secondary care. Although IgE sensitization increases in the first few years of life in children with eczema[8], the timing and pathogenic role of IgE sensitization in the development of atopic dermatitis remains uncertain[9]. Recent evidence strongly suggests that children with early-onset (<3 months) and more severe eczema have the greatest risk of IgE sensitization. Although debate remains as to the relative contributions of inherited barrier defects versus immunological aberrations, the major genetic risk identified to date is associated with loss-of-function mutations in *FLG*, encoding the skin barrier protein profilaggrin/filaggrin[2,4].

The spontaneous recessive mouse mutant flaky tail (ft) arose in 1958 on the background of an existing recessive hair phenotype, matted (ma), and since then has been maintained on a mixed strain[10]. Flaky tail mice have dry, flaky skin and annular tail and paw constrictions in the neonatal period[11]. Protein blot analysis shows that ft/ft mice express a truncated profilaggrin (~215 kDa) instead of the normal high-molecular-weight profilaggrin (>500 kDa)[11]. Although processed filaggrin in these mice has been shown to be virtually absent at the protein level[11], the underlying genetic mechanism is unknown. Given the likely genetic similarity between flaky tail mice and human ichthyosis vulgaris and atopic eczema, we sought to identify the genetic mechanism underlying this mutant and study in detail the function of the skin barrier in ft/ft mice with respect to ease of allergen priming.

The mouse filaggrin gene, *Flg*, is located on chromosome band 3QF2.1 within a cluster of seven genes encoding the fused S100 family of filaggrin-like proteins (**Fig. 1**). The organization of this cluster is identical to the orthologous human cluster. We manually annotated the intron-exon organization of the 20,150-bp *Flg* gene from the current build of the C57BL/6 mouse genome (**Fig. 1a** and **Supplementary Table 1** online). The genomic sequence derived from BAC clone RP23-227A12 contains small assembly errors owing to incomplete resolution of the tandem repeats within *Flg*. We resolved this issue by aligning individual filaggrin repeats and correcting the five detected assembly errors (**Supplementary Table 2** online) so that the complete ORF was in-frame with the reported short partial 5′ and 3′ cDNA sequences for mouse *Flg*[12,13]. The predicted 496-kDa mouse profilaggrin consists of 4,654 amino acids, including 16 full

[1]Institute of Molecular Medicine, Trinity College Dublin, Dublin, Ireland. [2]Department of Molecular Biology, Keio University School of Medicine, Tokyo, Japan. [3]Advanced Research Center for Genome Super Power, Keio University, Ibaraki, Japan. [4]Epithelial Genetics Group, Division of Molecular Medicine, Colleges of Life Sciences and Medicine, Dentistry & Nursing, University of Dundee, Dundee, UK. [5]Veterinary Sciences Centre, Conway Institute of Biomolecular and Biomedical Research, College of Life Sciences, University College Dublin, Dublin, Ireland. [6]Department of Dermatology, Keio University School of Medicine, Tokyo, Japan. [7]The Jackson Laboratory, Bar Harbor, Maine, USA. [8]Department of Oral Biology, School of Dentistry, University of Washington, Seattle, Washington, USA. [9]Division of Dermatology, Department of Medicine, University of Washington, Seattle, Washington, USA. [10]Department of Paediatric Dermatology, Our Lady's Children's Hospital, Crumlin, Dublin, Ireland. [11]These authors contributed equally to this work. Correspondence should be addressed to W.H.I.M. (w.h.i.mclean@dundee.ac.uk).

Received 11 September 2008; accepted 18 February 2009; published online 6 April 2009; doi:10.1038/ng.358

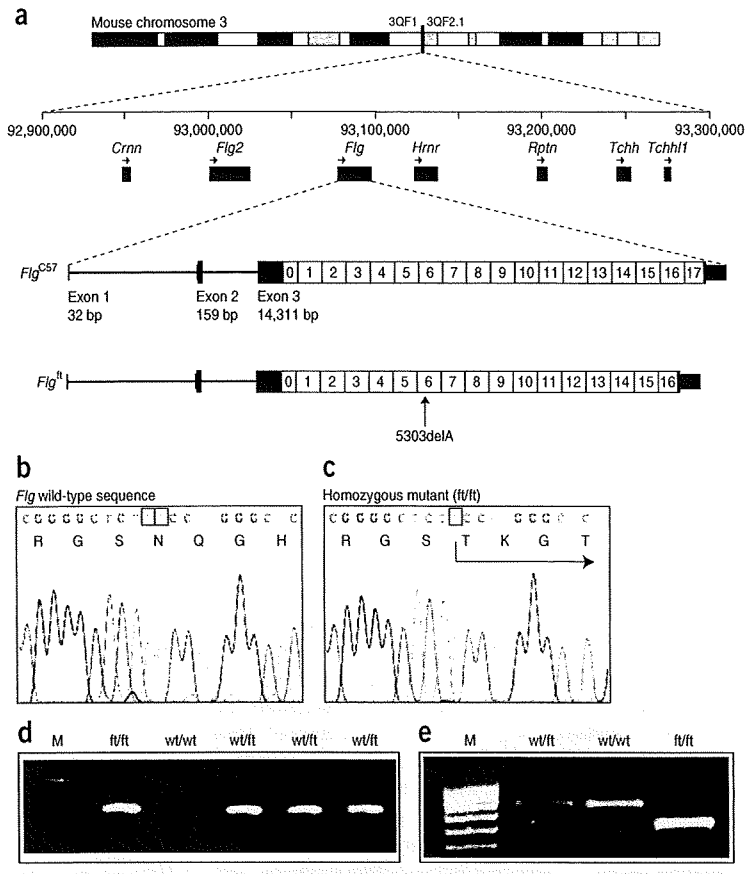

Figure 1 *Flg* gene structure and mutation identification. (**a**) *Flg* resides within a cluster of seven genes encoding closely related fused-S100 proteins, spanning ~350 kb on chromosomal band 3QF21. Like human *FLG*, mouse *Flg* has three exons. Exon 1 consists of 5′-UTR sequences only; exon 2 contains the ATG and encodes part of the N-terminal S100 calcium-binding domain of profilaggrin; and exon 3 encodes the remainder of the S100 domain, the B-domain and the filaggrin polyprotein repeat domain. In the July 2007 mouse genome sequence annotated here (Flg^{C57}), the latter consists of 16 near-perfect repeats encoding a 250-amino-acid filaggrin protein (1–16) flanked by two imperfect repeats (0 and 17). Repeat 17 is followed by a short tail domain. In ft mice, the exon 3 sequence (Flg^{ft}) lacks one repeat owing to a 750-bp in-frame deletion, as well as the frameshift mutation 5303delA. There are also several additional SNPs and small in-frame insertions/deletions in *Flg* that differ between the two strains; their DNA sequences overall are 99.3% identical, excluding the repeat copy number variation. (**b**) Wild-type *Flg*, corresponding to codons 1765–1771, with amino-acid translation. The A dinucleotide involved in the mutation is boxed. (**c**) Corresponding *Flg* sequence derived from a homozygous ft/ft mouse, showing the homozygous frameshift mutation designated 5303delA, predicting truncation sequence Asn1768ThrfsX154. The single A nucleotide remaining at the site of the mutation is boxed. (**d**) Allele-specific genotyping of the parents and F_1 offspring of a cross between an ft/ft homozygote and a wild-type mouse. M, molecular weight markers, upper band = 118 bp; lower band = 72 bp. The allele-specific band is only amplified from mice carrying the ft mutation. (**e**) Genotyping for an *Acc*I restriction site polymorphism in filaggrin repeat 1, approximately 4 kb upstream of the 5303delA mutation. The 678-bp C57BL/6 allele does not digest; the ft allele digests to yield fragments of 559 bp and 134 bp. M, molecular weight markers.

near-identical repeats of a 250-amino-acid filaggrin consensus sequence (repeats 1–16), flanked by two incomplete repeats (repeats 0 and 17; **Fig. 1a**). Most repeats are less than 1% different in protein sequence from each another. The amino terminus consists of a conserved S100 calcium-binding domain[14] and a B-domain postulated to have a signaling function[12,15]. The domain organization is identical to that of human profilaggrin[4], except that the mouse protein has 16 repeats of a smaller 250-amino-acid sequence versus 10–12 repeats of 324 amino acids in humans[4]. The number of repeats has been shown to vary among mouse strains[16], as it does in the human population[4,17]. Downstream of repeat 17 is a unique C-terminal domain. A polyclonal antibody raised against a synthetic peptide derived from the C-terminal tail domain recognized full-length ~500-kDa profilaggrin in wild-type mice, as well as intermediates from profilaggrin-to-filaggrin processing (**Fig. 2**), validating the predicted amino-acid sequence. Although traces of truncated profilaggrin (~215 kDa) can be seen in ft/ft homozygotes by total protein staining (**Fig. 2a**) and in protein blots using antibodies against a filaggrin repeat epitope, as previously reported[11], they are not recognized by the C-terminal antibody, predicting a truncating mutation (**Fig. 2b**).

Long-range PCR methods used to identify human *FLG* mutations[1,4] proved unable to amplify the larger exon 3 of mouse *Flg*. We therefore

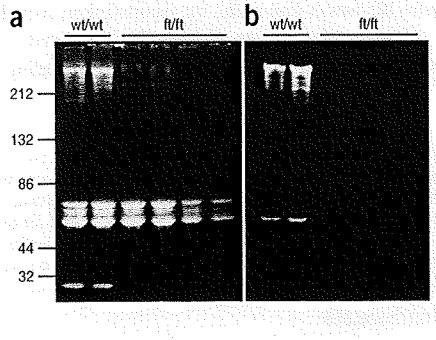

Figure 2 A truncated profilaggrin lacking the C terminus is expressed in flaky tail mouse skin. Urea/Tris protein extracts from wild-type and ft/ft mice were fractionated by SDS-PAGE and immunoblotted with a peptide antibody developed to the C terminus of mouse profilaggrin. (**a**) Coomassie brilliant blue–stained protein gel to control for loading. (**b**) Corresponding immunoblot probed with the C-terminal antibody. The antibody detects both full-length profilaggrin (P) and a putative C-terminal processing product (C) in wild-type mouse extracts; however, these immunoreactive products are not detected in ft/ft mice (**b**). Note the lack of filaggrin (F) in ft/ft mice (**a**), as observed previously[11]. The mutant profilaggrin protein in ft/ft mice is faintly visible in **a** at an apparent molecular weight of ~215 kDa (*). This is readily detectable with a mouse filaggrin antibody as reported previously[11]. Molecular weight marker sizes are shown at left.

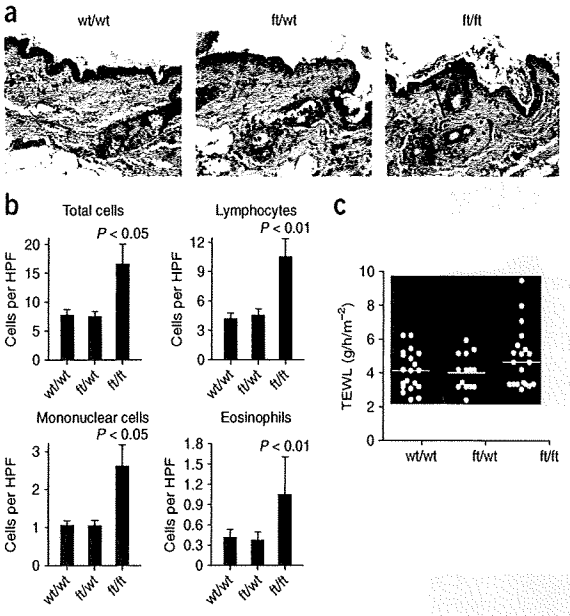

Figure 3 Cutaneous inflammation in untreated ft/ft mice but not wt/wt or wt/ft animals. (**a**) Representative photomicrographs of skin sections from age- and sex-matched wt/wt, wt/ft and ft/ft mice. Ft/ft mice had orthokeratotic hyperkeratosis (arrow) with occasional foci of acanthosis (bracket) compared to wt/wt and ft/wt mice (original magnification ×40). (**b**) Numbers of skin infiltrating cells, lymphocytes, eosinophils and mononuclear cells were detected per high-power field (HPF). Cells were counted on 15–20 HPF (×1,000) on hematoxylin and eosin–stained sections of 5–6 wt/wt, wt/ft and ft/ft mice. Data represent the mean; error bars represent s.e.m. Student's *t*-test, or corrected Welch corrected *t*-test, was used to determine statistical differences between groups. (**c**) TEWL analysis of untreated wt/wt, wt/ft and ft/ft mice. Values are individual mice, and mean bars are shown.

used a shotgun sequencing method whereby six species of short PCR fragments were generated and cloned using primers designed to amplify any of the repeat units, as recently used to detect human *FLG* mutations[18]. By sequencing >900 clones, we detected a 1-bp deletion in clones resulting from four different PCR fragments (**Fig. 1b,c**). Allele-specific PCR genotyping showed that this deletion completely cosegregated with the ft phenotype in many mouse crosses (**Fig. 1d**). We also detected an *Acc*I restriction fragment length polymorphism in filaggrin repeat 1 in tight linkage with the mutation. This marker proved to be convenient for genotyping ft mice, as heterozygotes are more easily scored than by allele-specific PCR (**Fig. 1e**). The ft mutation was subsequently backcrossed and maintained in our laboratories on the C57BL/6 background. Early in the course of backcrossing, we were able to remove the matted hair allele (ma) originally present on this mixed strain.

Given the nature of the shotgun method initially used, it was not possible to assemble the complete ft sequence for exon 3. However, we constructed a BAC library from an ft/ft homozygote and isolated a clone containing the entire *Flg* locus. We then subcloned exon 3 by recombineering and oversequenced by ~ninefold the resultant plasmid by random transposon insertion methodology. We sequenced exons 1 and 2 from ft/ft mice by standard PCR methods, allowing full assembly of the *Flg* sequence from the mutant strain. By this means, the mutation was unambiguously designated as 5303delA in filaggrin repeat 6, leading to premature termination 154 codons downstream (Asn1768ThrfsX154). The *Flg* sequence from ft mice was one filaggrin repeat shorter than the C57BL/6 sequence, consistent with earlier studies reporting variation in filaggrin repeat copy number both in mice and humans[4,17]. Otherwise, the coding sequence showed 99.3% identity between C57BL/6 and ft, with no other loss-of-function variants detected. Partial sequencing of *Flg* in different mouse strains suggested that the *Flg* locus in ft was originally derived from the C3H strain (data not shown).

We took skin biopsies for histopathological analysis from 6- to 8-week-old age- and sex-matched wt/wt (wild-type), wt/ft (heterozygous) and ft/ft (homozygous) mice. No overt differences were noted between wt/wt and wt/ft (**Fig. 3a**). In contrast, ft/ft mice had a mild diffuse orthokeratotic hyperkeratosis (a hypertrophy of the stratum corneum of the skin characterized by the presence of non-nucleated cells). We also observed occasional foci of acanthosis (abnormal thickening of the stratum spinosum layer of the skin), which varied in magnitude among individual ft/ft mice (**Fig. 3a**). In our hands, ft/ft mice have a phenotype consistent with the original description[11] but do not have significant acanthosis or alterations to the stratum granulosum as previously reported[11] possibly because histopathological analysis was done at a younger age. We observed a broad spectrum of severity of skin pathologies among individual ft/ft mice, including some with sporadic superficial dermal cellular infiltrates. We further characterized the cutaneous cellular infiltrate and, according to the number of cells detected per field (×1,000), we observed significantly more total cells ($P < 0.05$), lymphocytes ($P < 0.01$), eosinophils ($P < 0.05$) and mononuclear cells ($P < 0.01$) in ft/ft relative to wt/wt and wt/ft mice (**Fig. 3b**). To address the baseline integrity of the skin barrier of ft animals, we measured transepidermal water loss (TEWL) on the skin of adult age-matched wt/wt, wt/ft and ft/ft mice. Although there were higher individual TEWL readings in ft/ft mice, possibly reflecting the spectrum of severity in skin inflammation within this group, there was no statistically significant difference in baseline TEWL among the three groups (**Fig. 3c**).

To test allergen priming of the skin in these mice, we used the widely studied and clinically relevant allergen ovalbumin (OVA). We applied OVA or PBS (as a vehicle control) to the shaved abdominal skin of wt/wt, wt/ft and ft/ft mice (for full protocol, see **Supplementary Fig. 1a** online). Cutaneous exposure to OVA did not lead to gross skin lesions in any mice (data not shown). Skin removed from the site of allergen challenge showed evidence of some edema and a non-significant increase in cellular infiltrates but no gross damage or inflammation in wt/wt or ft/wt mice (**Fig. 4a,b**). In contrast, exposure of OVA to the skin of ft/ft mice induced diffuse mild acanthosis, with significant infiltrates of mixed, predominantly lymphocytic inflammatory cells, in addition to eosinophils and mononuclear cells (**Fig. 4a,b**). Measurement of TEWL at the site of allergen challenge 24 h after OVA application revealed a significant ($P < 0.0001$) elevation in TEWL of OVA-treated ft/ft mice relative to PBS-treated ft/ft and wt/wt and wt/ft mice (**Fig. 4c**). Application of OVA to wt/wt or wt/ft mice caused no alteration in TEWL (**Fig. 4c**).

We then analyzed the systemic immune response to OVA. Following cutaneous allergen exposure, wt/wt mice did not have elevated levels of total serum IgE, nor did they generate an antibody (IgG or IgE) response to OVA (**Fig. 5a** and **Supplementary Fig. 2** online), and spleen cells from wt/wt mice did not proliferate or produce cytokines when exposed to OVA *in vitro* (**Fig. 5b,c**). In contrast, percutaneous allergen exposure in ft/ft mice generated OVA-specific IgG and OVA-specific IgE that was significantly ($P > 0.005$) elevated relative to other PBS- or OVA-treated groups (**Fig. 5a**). The absence of allergen-specific responses in wt/wt mice upon allergen-challenge to

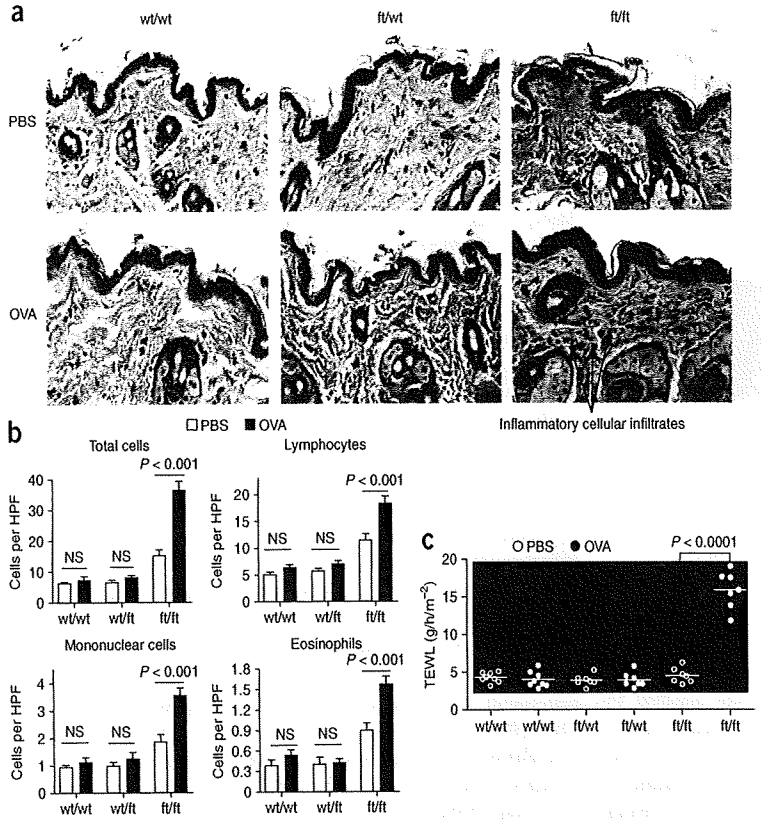

Figure 4 Allergen exposure exacerbates skin inflammation in ft/ft mice but not wt/wt or wt/ft animals. (**a**) Representative photomicrographs of skin sections from age- and sex-matched wt/wt, wt/ft and ft/ft mice exposed to OVA or PBS as a vehicle control. Ft/ft mice had diffuse mild acanthosis and marked increases in dermal cell infiltration when cutaneously challenged with OVA, compared to wt/wt and wt/ft mice (original magnification ×40). (**b**) Quantification of numbers of skin infiltrating cells, lymphocytes, eosinophils and mononuclear cells detected per high-power field (HPF). Cells were counted at on 15–20 HPF (×1,000) on hematoxylin and eosin–stained sections of 11–14 wt/wt, wt/ft and ft/ft mice. Data represent the mean; error bars represent s.e.m. Student's *t*-test, or corrected Welch corrected *t*-test, was used to determine statistical differences between groups. NS; nonsignificant. (**c**) TEWL analysis of skin of OVA-exposed wt/wt, wt/ft and ft/ft mice. Values relate to individual mice, and mean bars are shown.

intact skin has been reported previously in the background strain of the ft/ft mice used here (C57BL/6)[19]; however, an allergic response can be generated when OVA is applied after the skin barrier has been disrupted by tape-stripping[20]. Spleen cells from OVA-exposed ft/ft mice proliferated in a dose-dependent manner in response to OVA, whereas cells from other test groups did not proliferate (**Fig. 5b**). None of the PBS-treated groups developed OVA-specific cytokine responses in splenic cells (data not shown). Spleen cells from OVA-treated wt/wt and wt/ft mice did not secrete cytokines in response to OVA (**Fig. 5c**). In contrast, ft/ft mice produced OVA-specific Th2 (IL-4, IL-5, IL-13), Th1 (IFN-γ), regulatory (IL-10) and Th17 (IL-17) cytokines (**Fig. 5c**), indicating a generalized allergen-specific cytokine response that was not solely Th2 skewed. Consistent with a mixed T helper cytokine response in ft/ft mice treated with OVA cutaneously, there was elevation of serum levels of both OVA-specific IgG2a and IgG1, antibody isotypes that are induced by Th1 and Th2 cytokines, respectively[21] (**Supplementary Fig. 2b**). In these studies, wt/ft animals were comparable to wt/wt mice with respect to all parameters analyzed (**Figs. 3–5**).

These data show that ft/ft mice generate allergen-specific IgE and cytokine responses following cutaneous allergen challenge to intact skin. Several large studies have shown that *FLG* loss-of-function mutations predispose to asthma in the context of atopic dermatitis[5,22–24]. To experimentally address this association using the mouse model, we treated ft/ft and wt/wt animals that had been percutaneously treated with OVA with OVA aerosol to evoke pulmonary sensitization and airway hyper-responsiveness (AHR), and analyzed pulmonary responses (**Supplementary Fig. 1b**). AHR, determined as airway resistance (R_L), was not induced in OVA-exposed ft/ft or wt/wt mice, with both OVA-exposed groups having similar R_L values as PBS-exposed mice (**Supplementary Figs. 3** and **4** online). No airway inflammation was seen on lung histology sections from wt/wt or ft/ft mice exposed to OVA via the skin (**Supplementary Fig. 5a** online), which was subsequently confirmed and quantified by scoring histology sections (data not shown). Furthermore, there was no significant elevation in the numbers of total cells and eosinophils recovered in bronchoalveolar lavage (BAL) fluid between OVA-exposed or PBS-treated ft/ft and wt/wt mice (**Supplementary Fig. 5c,d**). OVA application to barrier-disrupted skin of wt/wt mice, as used to induce AHR on the more Th2 immunoreactive BALB/c strain previously[25], also failed to induce AHR in tape-stripped C57BL/6 mice (**Supplementary Fig. 4a**). The inability to induce AHR after cutaneous OVA challenge may thus reflect the use of C57BL/6 mice, which are less susceptible than BALB/c mice to allergen-induced Th2 inflammation.

To confirm that the OVA sensitization shown here in ft/ft is due to a specific defect in the skin barrier rather than a generalized altered immunity, we gave intraperitoneal injections of OVA and adjuvant (Alum) to ft/ft and wt/wt mice. We then evaluated allergen-specific responses (**Supplementary Fig. 3b** online). ft/ft mice intraperitoneally immunized with OVA and adjuvant developed allergen-specific immune responses comparable to wt/wt animals, with both groups developing a Th2-biased OVA-specific cytokine and antibody isotype response (**Supplementary Fig. 6** online).

To address whether the lack of pulmonary inflammation in ft/ft mice following allergen challenge was due to altered lung immunity and development of AHR in ft/ft mice, we challenged these animals and wt/wt mice intraperitoneally with OVA and adjuvant followed by pulmonary allergen sensitization (**Supplementary Fig. 3a**). There was comparable induction of AHR, determined as lung resistance (R_L), in wt/wt and ft/ft mice (**Supplementary Fig. 7** online). Furthermore, intraperitoneal challenge with OVA and adjuvant resulted in airway inflammation in both wt/wt and ft/ft mice (**Supplementary Fig. 5b**), with no differences between groups in the magnitude of lung inflammation detected (data not shown). Therefore ft/ft mice develop allergic lung inflammation after intraperitoneal priming with OVA and adjuvant but not when sensitized via the skin to OVA in the

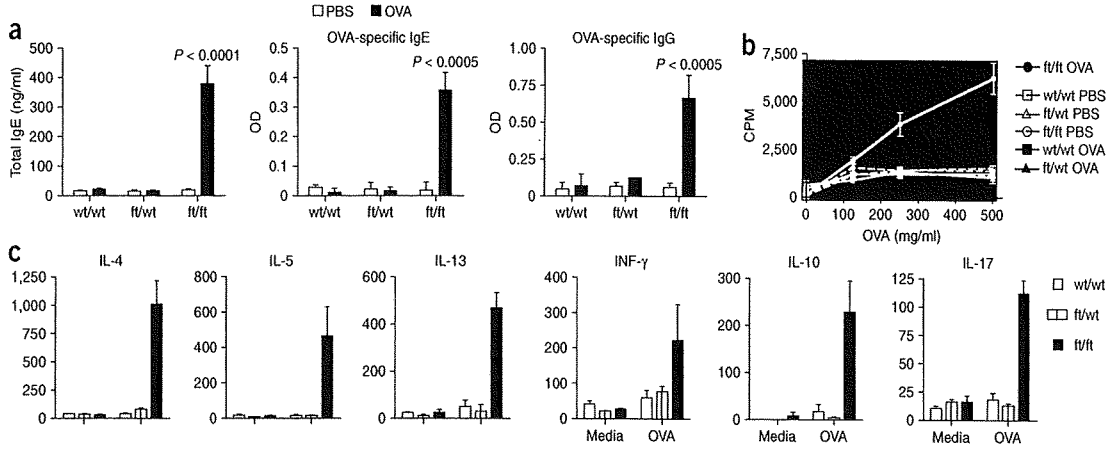

Figure 5 Elevated OVA-specific immune response in allergen exposed ft/ft mice but not wt/wt or wt/ft animals. (**a**) ELISA detection of levels of total IgE, OVA-specific IgE and IgG in serum from wt/wt, wt/ft and ft/ft mice treated with PBS or OVA on skin. Data are mean plus s.e.m. (from 7–12 mice). (**b**) Cell proliferation to OVA of spleen cells from wt/wt, wt/ft and ft/ft mice treated with PBS or OVA on skin. Data represent the mean of spleens from 3–4 individual mice per group; error bars represent s.e.m. (**c**) Cytokine production by spleen cells from OVA-exposed wt/wt, wt/ft and ft/ft mice treated with PBS or OVA. Cells were cultured in media or OVA (500 μg/ml) and cytokines detected by ELISA. Data represent the mean of spleens from 3–4 individual mice per group; error bars represent s.e.m. Student's *t*-test, or corrected Welch corrected *t*-test, was used to determine statistical differences between groups.

absence of adjuvant. Further work is needed to dissect whether this is due to the type of OVA-specific response generated in the absence of Alum, a Th2-inducing adjuvant, as opposed to the response generated following skin exposure to allergen in the absence of adjuvant.

Here we have identified the flaky tail mutation as a frameshift mutation 5303delA in repeat 6 of *Flg* (**Fig. 1**). Several truncating mutations have been reported in human *FLG*[4], including three in repeat 6. Notably, the truncated profilaggrin species resulting from mutations in repeats 7 and 10 of *FLG* have been shown to be highly unstable and incapable of being processed to functional filaggrin[4], as shown in the ft mouse here (**Fig. 2**) and previously[11]. Thus, the 5303delA mutation is a null allele, analogous to many of the human *FLG* mutations now emerging, and might be a better model for the human mutations than a knockout allele, which has proven difficult to generate owing to the repetitive nature of this locus (R.B.P. and W.H.I.M., unpublished data). Availability of genotyping assays for the mutant allele will allow generation of congenic strains and double mutant mice to further dissect the immunological and biological effects of *Flg* mutations.

Although ft/ft mice closely model the phenotypic, histological and ultrastructural characteristics of ichthyosis vulgaris in humans[11], we show here that these filaggrin-deficient mice are also predisposed to develop sensitization following percutaneous exposure to a model allergen, and develop cutaneous inflammatory infiltrates and allergen-specific immune responses following allergen sensitization (**Fig. 5**). Following sensitization, a further skin barrier defect, as measured by elevated TEWL, is seen, suggesting that the mild initial heritable barrier defect is exacerbated by allergic sensitization. This suggests that sensitization might also be an early event in filaggrin-deficient humans. Several known modifiers (for example, Th2 cytokines, including IL-13 and IL-4) have been shown to downregulate expression of filaggrin[26] and other key epidermal structural proteins[27], and unknown genetic factors may also influence the phenotype of ft/ft mice; these areas require further experimentation. It is noteworthy that PBS-treated ft/ft mice showed no elevation of total IgE up to 12–13 weeks of age (**Fig. 5**). Indeed, in 8-month-old untreated ft/ft mice, we have observed no increase in nonspecific IgE or elevated Th2 cytokine (IL-4, IL-5 and IL-13) production, and there are no previous reports of spontaneous atopy or eczema in ft/ft mice[10,11]. Thus, ft/ft mice maintained under specific pathogen-free conditions do not appear to develop spontaneous allergic responses, in contrast to NC/Nga mice[28].

As noted above, the role of elevated IgE in human atopic dermatitis remains unresolved. Given a recent report of a mouse model of intrinsic atopic eczema[29], which highlights the potential for eczema in mice in the absence of elevated IgE, caution is needed in assigning an obligate pathogenic role for elevated IgE in mouse atopic dermatitis. Although clarifying this relationship will require more experimentation on mouse models in addition to human studies, we have shown enhanced percutaneous priming in a mouse model of filaggrin deficiency that hints at possible mechanisms in the human disease. These findings set the scene for the use and further refinement of this animal model to further dissect the role of filaggrin in skin barrier function and the genesis of atopic eczema.

METHODS

Sequence analysis. We annotated the genomic sequence of the mouse *Flg* locus derived from BAC clone RP23-227A12 using the ClustalW tools within MacVector version 9.0. To identify the causative mutation in ft/ft mice, we applied the shotgun method recently developed to identify *FLG* mutations in humans with atopic dermatitis[18]. We used six pairs of PCR primers based on *Flg* exon 3 sequence on BAC clone RP23-227A12, designed to amplify each filaggrin homologous sequence unit (**Supplementary Table 3** online). The PCR products were cloned into the TA-cloning vector pGEM-tEasy (Promega). Plasmid DNA template was generated using the TempliPhi system (GE Healthcare Biosciences) and directly sequenced. We identified an identical 1-bp deletion of A in shotgun clones derived from four independent PCR fragments. To confirm the mutation and determine the full sequence of *Flg* from the mutant strain, we constructed a BAC library from homozygous ft/ft mice, which was screened by hybridization, and the resultant hits were confirmed by PCR (Amplicon Express). From a BAC containing the entire locus, we subcloned exon 3 into a plasmid vector by recombineering (Red/ET system, Gene Bridges). The subclone was subjected to random transposon insertion using the EZ-Tn5 <KAN-2> insertion kit (EPICENTRE Biotechnologies), and 96 transposon insertion clones were sequenced bidirectionally from the Tn5 insertion site, allowing full assembly of exon 3 with ~ninefold oversequencing.

Genotyping. For allele-specific PCR detection of the ft mutation, we amplified genomic DNA (2 ng) with primers mFlgdelA-F and mFlgdelA-R (**Supplementary Table 3**) using ×2 KOD FX PCR buffer containing 1.5 nmol $MgCl_2$, 0.2 U of KOD FX DNA polymerase (Toyobo Biochemicals). PCR amplification conditions were as follows: (94 °C, 2 min) ×1; (94 °C, 15 s; 70 °C, 30 s; 72 °C, 2 min) ×35; (72 °C, 5 min) ×1. PCR products were analyzed on 12% polyacrylamide gels. This PCR primer set is positive for ft/ft and wt/ft but negative for wt/wt (**Fig. 2d**). To more conveniently genotype animals, we developed a PCR assay to detect a 15-bp insertion polymorphism at the 5′ end of exon 3 in linkage disequilibrium with the ft mutation. This insertion creates an *Acc*I restriction site. We used primers FTins15.F and FTins15.R (**Supplementary Table 3**) in standard PCR reactions using the following amplification conditions: (94 °C, 5 min) ×1; (94 °C, 30 s; 58 °C, 30 s; 72 °C, 1 min) ×35; (72 °C, 5 min) ×1. Five microliters of PCR product were digested overnight with 2.5 U *Acc*I and resolved on 1.5% agarose gels. The 678-bp C57BL/6 allele does not digest; the ft allele digests to yield fragments of 559 bp and 134 bp (**Fig. 2e**).

C-terminal antibody. The C-terminal antibody specific for mouse profilaggrin was generated against the amino-acid sequence ESIFTAKHLDFNQSHS. The peptide was conjugated to KLH via an N-terminal cysteine residue before injection into New Zealand white rabbits (Genemed Synthesis). The serum was affinity purified before use. Urea/Tris extracts were prepared from newborn homozygous ft/ft mice and control C57BL/6 mice as described[11]. Protein samples were separated on 5–12% SDS/polyacrylamide gels and transferred to PVDF membrane (Millipore). Blots were probed with C-terminal antibody and immunoreactive proteins visualized with ECL (Amersham/GE Healthcare). A duplicate gel was stained with Coomassie Brilliant Blue R-250.

Mice. Breeding pairs of flaky tail (ft/ft) mice (original strain from Jackson Laboratory Stock a/a ma ft/ma ft/JSun; JR#9078; provided by J.P.S.) were backcrossed four generations onto a C57BL/6J strain background; C57BL/6J mice were used as wild-type (wt/wt) controls. Female mice were used in all experiments unless otherwise indicated. Flaky tail (ft/ft) mice were crossed with wild-type C57BL/6J mice to generate flaky tail heterozygous (wt/ft) mice. The OVA cutaneous sensitization experiments were repeated with F7 backcrossed mice, with littermates from wt/ft to wt/ft matings genotyped as wt/wt, wt/ft and ft/ft and used in experiments, giving identical results as the F4 backcross (data not shown). The mice were housed in SPF conditions, with irradiated diet and bedding provided. All animal experiments were done in compliance with Irish Department of Health and Children regulations and approved by the Trinity College Dublin's BioResources ethical review board.

Cutaneous challenge with OVA. We challenged the intact skin of wt/wt, wt/ft and ft/ft mice with OVA (Sigma Chemicals) by cutaneous exposure. We applied OVA in a regimen involving three cycles of daily exposure to OVA for 5 consecutive days (see **Supplementary Fig. 1a**). Abdominal hair was carefully shaved 24 h before application of OVA; mice with any visual damage to the skin were not used. OVA (fraction V; Sigma) was prepared in PBS (Dulbecco's PBS; Sigma) at 1 mg/ml. Mice were restrained and 50 µl of OVA solution, or 50 µl of PBS, was applied to the shaved skin and allowed to air dry. To address systemic allergen treatment, we challenged wt/wt and ft/ft mice with OVA in alum as an adjuvant by intraperitoneal injection as described[30] (see **Supplementary Fig. 3b**).

Measurement of trans-epidermal water loss (TEWL). We used a Courage and Khazaka Tewameter TM210 (Enviroderm) to measure TEWL. TEWL analysis of the abdomen of male and female adult (6–10 weeks of age) wt/wt and ft/ft mice occurred 24 h after shaving. Any mice with visual damage to the skin following shaving were not included in the analysis. TEWL was recorded at ambient temperature 19–21 °C and humidity 50% ± 5. In mice sensitized to OVA, TEWL was measured in PBS- and OVA-treated mice after OVA application.

Spleen cell preparation. Single-cell suspensions were prepared from spleens. Spleen cells were cultured in RPMI 1640 (Gibco-Invitrogen) supplemented with 10% (v/v) heat-inactivated FCS (FCS; Labtech), 2 mM L-glutamine (Gibco), 50 U/ml penicillin and 50 µg/ml streptomycin (Gibco). Spleen cells were plated at 5×10^6 cells/ml. OVA was subjected to endotoxin removal for use in cell assays as described[30]. Cells were unstimulated (media) or stimulated with OVA (250 and 500 µg/ml) in a 24-well plate (Greiner Bio-One) at 37 °C for 72 h. Supernatants were harvested after 72 h and cytokine levels (IL-4, IL-5, IL-13, IFN-γ, IL-10 and IL-17) were measured by ELISA. For cell proliferation analysis, cells were exposed to a range of concentrations of OVA in triplicate wells on 96-well plates. Cultures were pulsed with 1 µCi per well [^{3}H]thymidine (Amersham) for the last 14 h of culture. Cells were harvested with a cell harvester (Tomec) and [^{3}H]thymidine incorporation was measured by a Wallac β-counter (Perkin-Elmer).

Antibody and cytokine ELISA. Serum OVA-specific IgG, IgG1 and IgG2a levels were detected by direct ELISA using serial dilutions of sera. OVA-specific IgE was measured using biotinylated-OVA with 1:10 sera dilutions. Total serum IgE was measured using PharMingen antibodies (BD Biosciences), according to the manufacturer's instructions. We detected total serum IgG using commercial capture antibodies and IgG standard (Zymed Laboratories; Sigma). Sandwich ELISAs were done to quantify levels of specific cytokines in the supernatants cell cultures (IL-4, IL-5 and IL-13, assays supplied by PharMingen; IL-10, IL-17 and IFN-γ, assays supplied by R&D Systems).

Histology. Abdominal skin of age- and sex-matched mice (wt/wt, wt/ft and ft/ft) that were untreated or exposed to OVA was removed and fixed in 10% formaldehyde saline. Paraffin sections were stained with hematoxylin and eosin. Tissue sections were analyzed with slides blinded to genotype and exposure to allergen. To quantify the individual inflammatory cells infiltrating the skin, we used a previous described scoring system[20]. We counted the total number of cells, lymphocytes, eosinophils and mononuclear cells per ×1,000 high-power fields (HPF) of view, with 15–20 HPFs scored per mouse. Lungs were processed for histopathological analysis as described[30].

OVA challenge regimen for airway hyper-responsiveness (AHR). wt/wt and ft/ft mice were exposed to OVA cutaneously or intraperitoneally and then exposed to 20 min of continuous aerosol of 1% OVA each day for five consecutive days (as shown in **Supplementary Figs. 1b** and **3a**, respectively). Epicutaneous exposure to OVA was achieved by repeated tape-stripping of shaved skin[25] before OVA application using the regimen in **Supplementary Figure 1b**. AHR was analyzed the day following the final aerosol challenge. Mice were anesthetized, tracheostomized and ventilated. AHR was measured using a whole-body plethysmograph with a pneumotachograph linked to a transducer (EMMS). The average lung resistence (R_L) and the area under the resistence curve (R_L AUC) parameters were quantified for 3-min periods at baseline and after exposure to nebulized endotoxin-free PBS (Sigma) and acetyl-β-methycholine chloride (Sigma) at 10, 30, 60 and 120 mg/ml. Broncho-alveolar lavage (BAL) fluids were collected by canulating the trachea and lavaging the lungs with a 1.0 ml of ice-cold PBS. BAL cells were pelleted, washed and counted. The numbers of eosinophils in BAL were analyzed by flow cytometry as described[30]. Lungs were removed from mice for histology.

Statistics. All animal experiments were repeated at least twice. GraphPad Prism and GraphPad Instat software were used for data analysis. Difference between groups was determined by Student's *t*-test or, if nonparametric, Welch corrected *t*-test. Differences were considered significant when $P < 0.05$.

Accession codes. BAC clone RP23-227A12, AC158361; 5′ *Flg*, AF510860; 3′ *Flg*, J03458; *Flg* complete sequence from ft mouse strain, FJ824603.

Note: Supplementary information is available on the Nature Genetics website.

ACKNOWLEDGMENTS

We thank B. Mistry, A. Smyth, T. Adachi and M. Furuhashi for their technical assistance and T. Yoshida for his cooperation. We are grateful for the assistance of B. Cloak with photomicrography and S. Worrell with histopathology. This work was supported by the Labour Sciences Research Grants for Research on Allergic Disease and Immunology from the Ministry of Health, Labour, and Welfare of Japan (M.A.), National Institute of Health grants P01 AM21557 (P.F.), R01 AR49183 (R.B.P.) and the Odland Endowed Research Fund (P.F.). P.G.F. was supported by Science Foundation Ireland. A.D.I. is supported by the Children's Medical and Research Foundation, OLCHC. Filaggrin research in the McLean laboratory is supported by grants from The British Skin Foundation, The National Eczema Society, The Medical Research Council (Reference number G0700314) and donations from anonymous families affected by eczema in the Tayside Region of Scotland.

AUTHOR CONTRIBUTIONS

The study was designed by W.H.I.M., P.G.F., A.D.I and M.A. Molecular biology was performed by T.S., A. Sandilands, L.E.C., H.K., A. Shiohama, A.K., N.S. and J.K. Bioinformatics was performed by W.H.I.M. C-terminal profilaggrin antibody and immunoblot data was generated by R.B.P. and P.F. The initial mixed strain ft mice were provided by J.P.S. Mouse backcrossing, immunology and histological experiments were performed by P.G.F., S.P.S., N.E.M and J.J.C. The manuscript was written by P.G.F., T.S., J.K., M.A., R.B.P., A.D.I. and W.H.I.M.

Published online at http://www.nature.com/naturegenetics/
Reprints and permissions information is available online at http://npg.nature.com/reprintsandpermissions/

1. Smith, F.J.D. *et al.* Loss-of-function mutations in the gene encoding filaggrin cause ichthyosis vulgaris. *Nat. Genet.* **38**, 337–342 (2006).
2. Palmer, C.N.A. *et al.* Common loss-of-function variants of the epidermal barrier protein filaggrin are a major predisposing factor for atopic dermatitis. *Nat. Genet.* **38**, 441–446 (2006).
3. Baurecht, H. *et al.* Toward a major risk factor for atopic eczema: meta-analysis of filaggrin polymorphism data. *J. Allergy Clin. Immunol.* **120**, 1406–1412 (2007).
4. Sandilands, A. *et al.* Comprehensive analysis of the gene encoding filaggrin uncovers prevalent and rare mutations in ichthyosis vulgaris and atopic eczema. *Nat. Genet.* **39**, 650–654 (2007).
5. Henderson, J. *et al.* The burden of disease associated with filaggrin mutations: a population-based, longitudinal birth cohort study. *J. Allergy Clin. Immunol.* **121**, 872–877 (2008).
6. Williams, H. & Flohr, C. How epidemiology has challenged 3 prevailing concepts about atopic dermatitis. *J. Allergy Clin. Immunol.* **118**, 209–213 (2006).
7. Spergel, J.M. & Paller, A.S. Atopic dermatitis and the atopic march. *J. Allergy Clin. Immunol.* **112**, S118–S127 (2003).
8. Illi, S. *et al.* The natural course of atopic dermatitis from birth to age 7 years and the association with asthma. *J. Allergy Clin. Immunol.* **113**, 925–931 (2004).
9. Bieber, T. Atopic dermatitis. *N. Engl. J. Med.* **358**, 1483–1494 (2008).
10. Sundberg, J.P. in *Handbook of Mouse Mutations with Skin and Hair Abnormalities. Animal Models and Biochemical Tools.* Vol. 2 (ed. Sundberg, J.P.) *The flaky tail (ft) mutation*, 269–273 (CRC Press, Ann Arbor, Michigan, USA, 1984).
11. Presland, R.B. *et al.* Loss of normal profilaggrin and filaggrin in flaky tail (ft/ft) mice: an animal model for the filaggrin-deficient skin disease ichthyosis vulgaris. *J. Invest. Dermatol.* **115**, 1072–1081 (2000).
12. Pearton, D.J., Dale, B.A. & Presland, R.B. Functional analysis of the profilaggrin N-terminal peptide: identification of domains that regulate nuclear and cytoplasmic distribution. *J. Invest. Dermatol.* **119**, 661–669 (2002).
13. Rothnagel, J.A., Mehrel, T., Idler, W.W., Roop, D.R. & Steinert, P.M. The gene for mouse epidermal filaggrin precursor. Its partial characterization, expression, and sequence of a repeating filaggrin unit. *J. Biol. Chem.* **262**, 15643–15648 (1987).
14. Presland, R.B., Bassuk, J.A., Kimball, J.R. & Dale, B.A. Characterization of two distinct calcium-binding sites in the amino-terminus of human profilaggrin. *J. Invest. Dermatol.* **104**, 218–223 (1995).
15. Zhang, D., Karunaratne, S., Kessler, M., Mahony, D. & Rothnagel, J.A. Characterization of mouse profilaggrin: evidence for nuclear engulfment and translocation of the profilaggrin B-domain during epidermal differentiation. *J. Invest. Dermatol.* **119**, 905–912 (2002).
16. Rothnagel, J.A. & Steinert, P.M. The structure of the gene for mouse filaggrin and a comparison of the repeating units. *J. Biol. Chem.* **265**, 1862–1865 (1990).
17. Gan, S.Q., McBride, O.W., Idler, W.W., Markova, N. & Steinert, P.M. Organization, structure, and polymorphisms of the human profilaggrin gene. *Biochemistry* **29**, 9432–9440 (1990).
18. Sasaki, T. *et al.* Sequence analysis of filaggrin gene by novel shotgun method in Japanese atopic dermatitis. *J. Dermatol. Sci.* **51**, 113–120 (2008).
19. Terada, M. *et al.* Contribution of IL-18 to atopic-dermatitis-like skin inflammation induced by *Staphylococcus aureus* product in mice. *Proc. Natl. Acad. Sci. USA* **103**, 8816–8821 (2006).
20. Spergel, J.M., Mizoguchi, E., Oettgen, H., Bhan, A.K. & Geha, R.S. Roles of TH1 and TH2 cytokines in a murine model of allergic dermatitis. *J. Clin. Invest.* **103**, 1103–1111 (1999).
21. Snapper, C.M. & Paul, W.E. Interferon-gamma and B cell stimulatory factor-1 reciprocally regulate Ig isotype production. *Science* **236**, 944–947 (1987).
22. Weidinger, S. *et al.* Filaggrin mutations, atopic eczema, hay fever, and asthma in children. *J. Allergy Clin. Immunol.* **121**, 1203–1209 (2008).
23. Marenholz, I. *et al.* Filaggrin loss-of-function mutations predispose to phenotypes involved in the atopic march. *J. Allergy Clin. Immunol.* **118**, 866–871 (2006).
24. McLean, W.H.I. *et al.* Filaggrin variants confer susceptibility to asthma. *J. Allergy Clin. Immunol.* **121**, 1294–1295 (2008).
25. Spergel, J.M. *et al.* Epicutaneous sensitization with protein antigen induces localized allergic dermatitis and hyperresponsiveness to methacholine after single exposure to aerosolized antigen in mice. *J. Clin. Invest.* **101**, 1614–1622 (1998).
26. Howell, M.D. *et al.* Cytokine modulation of atopic dermatitis filaggrin skin expression. *J. Allergy Clin. Immunol.* **120**, 150–155 (2007).
27. Kim, B.E., Leung, D.Y., Boguniewicz, M. & Howell, M.D. Loricrin and involucrin expression is down-regulated by Th2 cytokines through STAT-6. *Clin. Immunol.* **126**, 332–337 (2008).
28. Matsuda, H. *et al.* Development of atopic dermatitis-like skin lesion with IgE hyperproduction in NC/Nga mice. *Int. Immunol.* **9**, 461–466 (1997).
29. Chen, L., Overbergh, L., Mathieu, C. & Chan, L.S. The development of atopic dermatitis is independent of Immunoglobulin E up-regulation in the K14-IL-4 SKH1 transgenic mouse model. *Clin. Exp. Allergy* **38**, 1367–1380 (2008).
30. Mangan, N.E., van Rooijen, N., McKenzie, A.N. & Fallon, P.G. Helminth-modified pulmonary immune response protects mice from allergen-induced airway hyperresponsiveness. *J. Immunol.* **176**, 138–147 (2006).

Published

JEM

Brief Definitive Report

External antigen uptake by Langerhans cells with reorganization of epidermal tight junction barriers

Akiharu Kubo,[1,2] Keisuke Nagao,[1,2] Mariko Yokouchi,[1] Hiroyuki Sasaki,[3,4] and Masayuki Amagai[1]

[1]Department of Dermatology and [2]Center for Integrated Medical Research, School of Medicine, Keio University, Tokyo 160-8582, Japan
[3]Department of Molecular Cell Biology, Institute of DNA Medicine, Jikei University School of Medicine, Tokyo 105-8461, Japan
[4]The Center for Advanced Medical Engineering and Informatics, Osaka University, Osaka 565-0871, Japan

Outermost barriers are critical for terrestrial animals to avoid desiccation and to protect their bodies from foreign insults. Mammalian skin consists of two sets of barriers: stratum corneum (SC) and tight junctions (TJs). How acquisition of external antigens (Ags) by epidermal Langerhans cells (LCs) occur despite these barriers has remained unknown. We show that activation-induced LCs elongate their dendrites to penetrate keratinocyte (KC) TJs and survey the extra-TJ environment located outside of the TJ barrier, just beneath the SC. Penetrated dendrites uptake Ags from the tip where Ags colocalize with langerin/Birbeck granules. TJs at KC–KC contacts allow penetration of LC dendrites by dynamically forming new claudin-dependent bicellular- and tricellulin-dependent tricellular TJs at LC–KC contacts, thereby maintaining TJ integrity during Ag uptake. Thus, covertly under keratinized SC barriers, LCs and KCs demonstrate remarkable cooperation that enables LCs to gain access to external Ags that have violated the SC barrier while concomitantly retaining TJ barriers to protect intra-TJ environment.

CORRESPONDENCE
Akiharu Kubo:
akiharu@a5.keio.jp

Abbreviations used: 3D, three-dimensional; Ag, antigen; bTJ, bicellular TJ; KC, keratinocyte; LC, Langerhans cell; pAb, polyclonal antibody; SC, stratum corneum; SG, stratum granulosum; TJ, tight junction; tTJ, tricellular Tj; ZO-1, zonula occludens 1.

Although mucus covers the epidermis in fish and amphibian tadpoles, terminally differentiated cornified cellular sheets called the stratum corneum (SC) constitute the outmost epidermal layer in amphibian adults, reptiles, birds, and mammals and serve as a physical barrier to protect the living layer underneath (Madison, 2003). Beneath the mucus or SC, apical intercellular spaces of the living stratified epidermal cells are sealed with tight junctions (TJs) that limit paracellular leakage of water and electrolytes to maintain fluid homeostasis (Furuse et al., 2002; Tsukita and Furuse, 2002). The existence of TJ barriers in epidermis has been reported in fish, amphibians, reptiles, and, recently, in mammals (Farquhar and Palade, 1965; Mittal and Whitear, 1979; Landmann et al., 1981; Brandner et al., 2002). The knockout study of claudin-1, a TJ-specific integral membrane protein, demonstrated that TJs function as paracellular diffusion barriers in mammalian epidermis (Furuse et al., 2002). The lack of a wide-area visualization method for TJ honeycomb structures in skin, however, has hampered further detailed analysis.

Skin is a major entry site for microbial pathogens and allergens and is heavily guarded by DCs, leukocyte subsets which regulate immunity. Langerhans cells (LCs), which represent the most studied skin DCs and have been reported to elicit immune responses against foreign antigens (Ags) in vivo (Merad et al., 2008; Nagao et al., 2009), exist in the epidermis and, thus, are in the best position to encounter foreign Ags. LCs elongate their dendrites between keratinocytes (KCs) to comprise a dense network that covers the entire body surface. Routes of entrance for Ags, which are taken up by skin DCs, have not received attention in relation to skin barriers. Despite the discovery of mammalian epidermal TJs that had long been overlooked, this barrier is still totally neglected, and it is taken for granted that skin DCs have access to pathogens or allergens that have somehow

The Rockefeller University Press $30.00
J. Exp. Med. Vol. 206 No. 13 2937-2946
www.jem.org/cgi/doi/10.1084/jem.20091527

Supplemental Material can be found at:
http://jem.rupress.org/cgi/content/full/jem.20091527/DC1

entered the skin at the time of Ag uptake (McGrath and Uitto, 2008; Oyoshi et al., 2009). In this study, we demonstrate that activated LCs gain access to extra-TJ Ags by sending their dendrites out through epidermal TJs. TJ at KC–KC contacts allowed penetration of LC dendrite but maintained TJ barrier integrity by reorganizing new TJ at LC–KC contacts. Our study in stratified epithelium reveals a remarkably orchestrated system for Ag uptake and barrier maintenance that occurs at the forefront of external–internal interface in skin.

RESULTS AND DISCUSSION

Three-dimensional (3D) visualization of epidermal TJs and LCs

To study the functional interaction between the physical epidermal barrier and immunological surveillance system, we first enabled 3D visualization of TJs in epidermal sheets (Fig. 1 A and Video 1). 3D reconstruction images confirmed that the stratum granulosum (SG) is composed of three flattened KC cellular sheets (SG1, SG2, and SG3 cells, from top to bottom; Furuse et al., 2002; Tsuruta et al., 2002), and zonula occludens 1 (ZO-1) staining demonstrated that TJs seal the paracellular pathway between SG2 cells (Fig. 1 B and Video 1). Claudin-1 staining concentrated with ZO-1 in TJs but was diffuse on basolateral surfaces of SG2 cells and total cell surfaces of SG3 cells (Fig. 1 B and Video 1), which is concordant with previous results in vertical sections (Furuse et al., 2002). Note that SG1 cells are claudin-1 negative and exist outside of TJ barriers (Fig. 1 B; Video 1; and see Fig. 5 D).

We next evaluated the positioning of LC dendrites in relation to TJs. LCs could be visualized in conjunction with TJs in epidermal sheets with antibodies against ZO-1, claudin-1, and class II MHC (MHC II). MHC II was observed to accumulate in the perinuclear area of LCs (Fig. 1 C), suggesting that these LCs were in a resting state (Aiba and Katz, 1990). Claudin-1 staining exhibited a faint but well contrasted staining of TJs (Fig. 1 C, slice 7–23) and exhibited bright staining on the surface of LC cell bodies in the deep epidermis (Fig. 1 C, slice 43–51), which is consistent with previous FACS analysis reporting claudin-1 expression on LCs (Zimmerli and Hauser, 2007). 3D reconstruction images demonstrated an upward projection of LC dendrites toward the skin surface, which stopped short of the SG2 layer with obvious spaces between dendrite tips and TJs (Fig. 1 D and Video 2).

Activated LCs elongate their dendrites through TJ

We then investigated the relationship between TJs and dendrites of activated LCs. Upon sensing inflammatory signals, LCs exhibit a series of coordinated changes, including increases in size, dSEARCH motion of dendritic processes, upregulation of surface MHC II, and subsequent migration to draining lymph nodes (Thomas et al., 1980; Larsen et al., 1990; Nishibu et al., 2006). As LC activation is readily inducible in vivo by tape stripping (Streilein et al., 1982), we investigated the effect of tape stripping on TJs and LCs. SG1 cells and a significant portion of the SC remained intact after the tape-strip procedure as determined by confocal and electron microscopy (unpublished data). Tape stripping induced clusters of LCs to express high levels of surface MHC II within 12 h (Fig. S1 A and Fig. 2 A). We noticed that many ZO-1^{high} spots were induced on TJs but were limited to those that overlaid MHC II^{high} LCs (Fig. 2 A). High-magnification imaging of these ZO-1^{high} spots revealed that MHC II^{high} LC dendrites docked with TJs, indicating that the dendrite tips were exposed to extra-TJ environments of the SG1 layer (Fig. 2, B–E). Strikingly, some LC dendrites penetrated through TJs to reach to the bottom of the SC (Fig. 2 C and Video 2). TJ docking or penetrating dendrites showed particularly high expression of ZO-1 and claudin-1 along their dendrites within the SG2 layer (Fig. 2, C–E), strongly suggesting that TJs are formed between LC dendrites and surrounding SG2 cells, presumably to retain TJ barrier integrity. After 12 h of tape stripping, the vast majority of activated LCs displayed one to four dendrites that had either docked or penetrated TJs (Fig. 2 G), both in ear and trunk skin (Fig. S2), indicating that intraepidermal activation of LCs almost always involves trans-TJ penetration of LC dendrites. Interestingly, LC dendrites have been reported to become highly mobile after tape stripping (Kissenpfennig et al., 2005; Nishibu et al., 2006), indicating that activated LCs search paracellular spaces actively to dock their dendrites with TJs to reach the extra-TJ environment. Dendrite tips could sometimes be observed spreading horizontally between SG1 and SG2 cells after penetrating TJs, in which lamellipodia-like membrane protrusions were observed (Fig. 2 F), further suggesting that LC dendrites continue to search paracellular spaces after TJ penetration.

Next, we evaluated whether TJ docking and penetration of LCs occurred in response to cytokine signals. TNF and IL-1β have been reported to be KC-derived proinflammatory cytokines rapidly induced by tape stripping (Wood et al., 1992) and leading to LC activation and dSEARCH motion (Enk et al., 1993; Nishibu et al., 2007). As expected, subcutaneous injection of TNF or IL-1β, but not PBS, induced numerous clusters of MHC II^{high} LCs within 12 h (Fig. S1 B). Again, these activated LCs uniformly exhibited TJ docking or penetration, and the number of TJ-docked dendrites was similar to that induced by tape stripping (Fig. S1 C). These observations demonstrated that TJ docking and penetration is a common feature for LCs that have undergone intraepidermal activation at least in an acute phase. Interestingly, genomic knockout of CX3CR1, which has been reported to mediate DC access to the intestinal lumen beyond TJs in lamina propria (Niess et al., 2005), failed to suppress tape stripping–induced TJ docking or penetration by LCs (unpublished data), suggesting the existence of unknown signals that remain to be identified.

Some LC dendrites were reported to end just beneath the SC, forming button-like structures in humans (Langerhans, 1868; Ferreira-Marques, 1951). Our study also showed that the dendrite tips at the TJ-docking site sometimes displayed button-like structures (Fig. 2 E). Perhaps the previous observations made by these LC pioneers were dendrites of activated LCs that had docked with TJs.

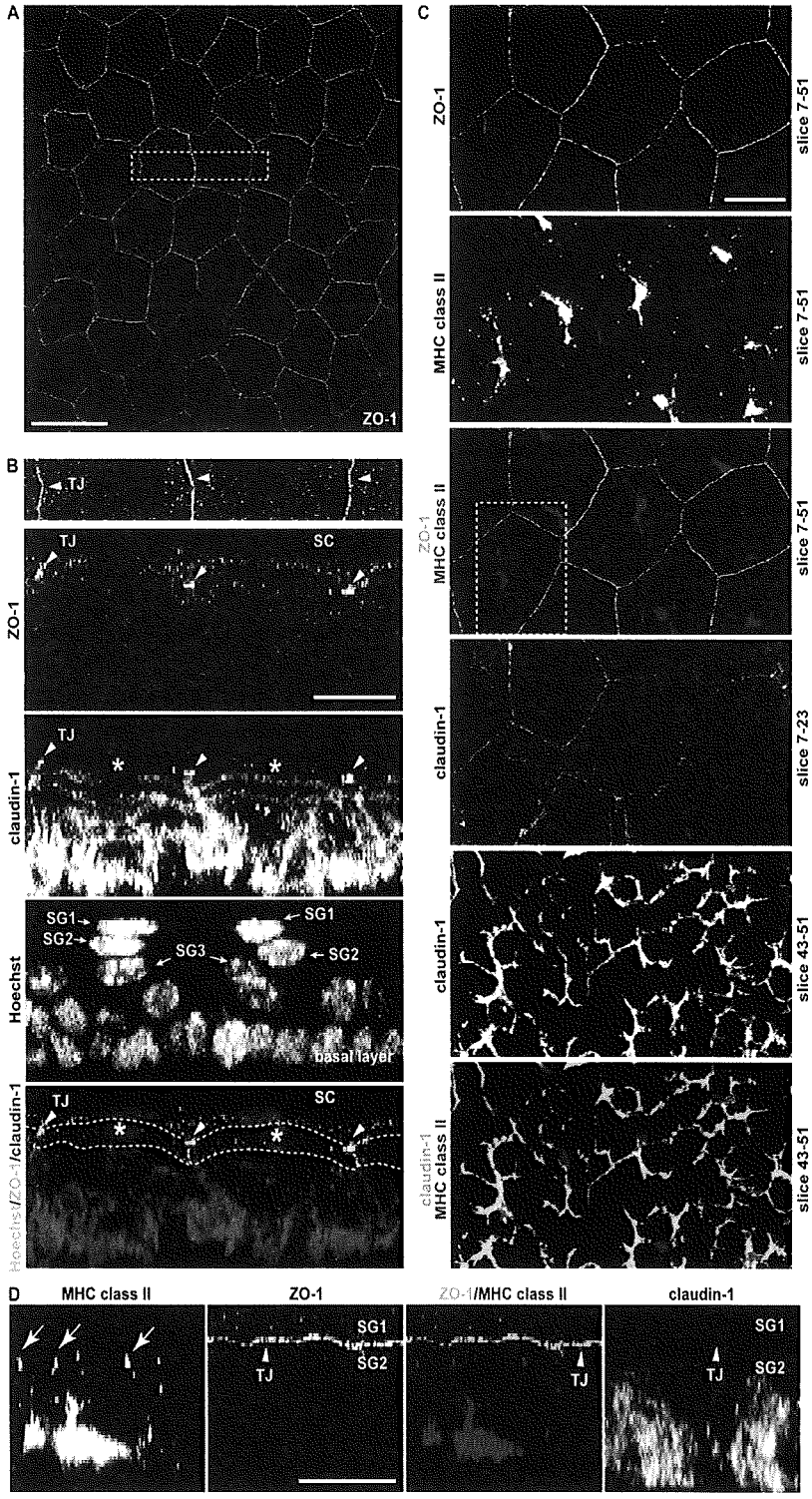

Figure 1. 3D visualization of epidermal TJs and LCs. (A) TJ network visualized by anti-ZO-1 antibody in epidermal sheet demonstrated en face by confocal microscopy. Bar, 50 µm. (B) A 90° rotation image of the boxed area in A. The top shows an en face image of ZO-1 staining followed by rotation images stained for the indicated TJ molecules. Among the three layers of granular layer, SG1 to SG3, TJs (arrowheads) were found exclusively in the SG2 layer (asterisk and dashed lines), and rotation images display TJs as bright dots with intense ZO-1 and claudin-1 signals (see Video 1). (C) TJs and LCs in unperturbed skin. Z-slice numbers are indicated in each panel. ZO-1 and claudin-1 colocalized at KC–KC TJs, and LCs (MHC II$^+$) coexpressed claudin-1 at high levels. (D) A 90° rotation image of the boxed area in C (see Video 2). Tips of LC dendrites (arrows) localized within TJ barriers (arrowheads). Bars, 20 µm. Data presented is representative of five mice.

Published

JEM

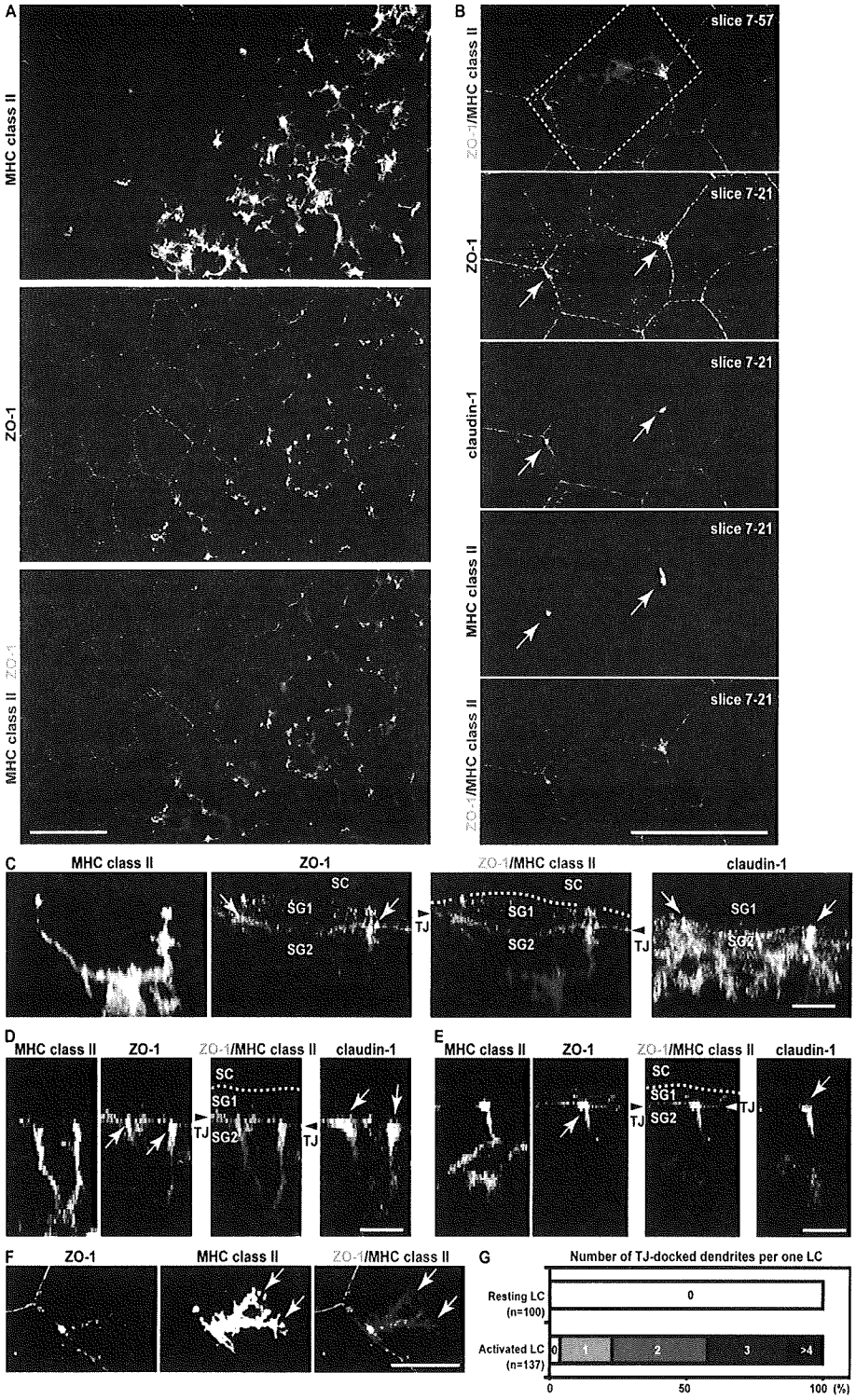

Figure 2. TJ docking and penetration by activated LCs. (A) Activated LCs exhibit brighter surface MHC II compared with resting LCs. ZO-1^{high} spots identify where LC dendrites dock with TJs. (B) TJ penetration by activated LC dendrites (see Video 2) and accumulation of ZO-1 and claudin-1 at penetration points (arrows). Z-slice numbers are indicated in each panel. (C–F) Various forms of TJ docking and penetration. A 90° rotation of the boxed area in B is shown in C. Dashed lines indicate the SC–SG1 interface. Dendrites penetrated (C, arrows) or docked with (D, arrows) TJs, formed button-like structures (E, arrows), or formed lamellipodia-like protrusions (F, arrows) elongating horizontally between SG1 and SG2 cells after penetrating TJs. Bars: (A and B) 50 µm; (C–F) 10 µm. (G) Numbers of TJ-docked dendrites per cell on resting or activated LC after 12 h of tape stripping. Data presented in A–F is representative of five mice, and data in G of three independent experiments.

TJ reorganization prevents TJ leakage at LC penetration points

Penetration of TJs at KC–KC contacts by LC dendrites presumably requires focal reorganization of TJ barriers that seal SG2 cells as well as concomitant formation of TJs at LC–KC contacts to minimize TJ leakage. TJ barriers in simple epithelia consist of bicellular TJs (bTJs) that seal intercellular space between two adjacent epithelial cells and tricellular TJs (tTJs) that form three pairs of vertically extended TJs at tricellular contacts (Fig. 3 A; Staehelin, 1973; Ikenouchi et al., 2005). Tricellulin is a transmembrane protein exclusively localized to tTJs and is indispensable for proper TJ barrier function (Ikenouchi et al., 2005). We determined that tricellulin also concentrates at tricellular points of TJs in stratified epithelia in vivo, further highlighting the importance of tTJs as a component of TJ barriers (Fig. 3, B and C). We hypothesized that if TJ integrity is maintained at TJ docking or penetrating sites, new tricellular contacts that form between an LC dendrite and two neighboring SG2 cells should be sealed by tTJs. Three patterns for docking could be modeled (Fig. 3 D, 1–3). Indeed, careful examination of TJ docking or penetration revealed all three patterns. In pattern 1 (Fig. 3 D, 1), in which dendrite penetrations were seen through KC–KC bTJs, two new sets of vertically extended LC–KC tTJs were revealed by tricellulin staining (Fig. 3 E and Video 3). In pattern 2, in which LC dendrites penetrate a preexisting KC–KC tricellular contact (Fig. 3 D, 2), three new LC–KC tTJs are positioned at nearly 120° intervals also on the newly formed LC-KC bTJ ring and extend vertically below (Fig. 3 F and Video 3). In pattern 3, a variation of pattern 2 (Fig. 3 D, 3), one vertical extension of tTJs managed to bring together four contact points (Fig. 3 G). The frequency of penetration through bicellular or tricellular KC–KC contacts was similar (Fig. 3 H). These observations strongly suggest that LCs and KCs actively interact with each other to strictly regulate the integrity of epidermal TJs during TJ penetration.

TJ-penetrated dendrites engage in endocytosis

We next sought to address the biological significance of TJ penetration. If LCs uptake foreign material such as microbial pathogens before actual invasion without disabling the TJ barrier, it would be advantageous to the host. To address this, we investigated whether LCs could engage in endocytic activity via dendrite tips that have penetrated TJs. Langerin-positive Birbeck granule is an endocytic receptor that is, so far, unique to LCs (Valladeau et al., 2000). Langerin is a C-type lectin that binds mannose and related sugars in a calcium-dependent manner and has also been reported to mediate internalization of OVA and HIV (Valladeau et al., 2003; Takahara et al., 2004; Merad et al., 2008). We found that langerin accumulated in dendrite tips of activated LCs but not in resting LCs (Fig. 4 A), indicating that Birbeck granule formation is prominent in activated LC dendrites.

To analyze endocytic activity, we topically applied a protein biotinylation reagent, sulfo-NHS-LC-biotin, on mouse ear skin. This reagent is membrane impermeable and epidermal TJ unpenetrable (Furuse et al., 2002). Remarkably, 16 h after application, biotin signals accumulated within dendrites of activated LCs that were limited to those that had penetrated TJs (Fig. 4 B and Video 4). Biotin signals were observed as a streak starting from the tip through the center of the dendrites (Fig. 4 C and Video 4), indicating that active endocytosis takes place at the tip, and there exists a continuous membrane flow to the cell body. A significant part of biotin signals within dendrites colocalized with langerin (Fig. 4 D), indicating that Birbeck granules take part in this endocytic machinery.

LCs uptake extra-TJ Ags

Previous in vitro studies demonstrated that langerin could mediate uptake of OVA (Takahara et al., 2004). To directly determine that the endocytic machinery described in the previous section is associated with Ag uptake, we examined whether LCs were capable of acquiring foreign Ags in vivo using FITC-OVA. Because an aqueous FITC-OVA solution failed to pass through the SC by simple topical application, we applied it using an occlusive dressing. TJ is a size-selective barrier. In good agreement with this, a 45-kD FITC-OVA signal was not observed in the living layer of epidermis (Fig. 4 E). Strikingly, FITC-OVA was observed to accumulate within the LC dendrites that penetrated TJs but not within dendrites that stayed below TJ barrier, even in activated LCs (Fig. 4, E and F). In TJ-penetrated LCs, langerin colocalized with FITC-OVA signal that displayed as streaks in dendrites and as perinuclear accumulations, strongly suggesting that FITC-OVA may be endocytosed via Birbeck granules at the tip and transported by intracellular trafficking (Fig. 4 E and Video 4). Application of GFP-expressing *Escherichia coli* resulted in strong GFP signal in TJ-penetrating dendrites, indicating that skin surface microbes or associated Ags could also be captured (Fig. 4 G).

Finally, we performed electron microscopy using lanthanum nitrate to confirm the existence of Birbeck granules at TJ-penetrating tips and to confirm the integrity of TJs where penetration occurs (Fig. 5, A–C). The lanthanum penetration assay is an established method to evaluate TJ permeability (Hashimoto, 1971; Shaklai and Tavassoli, 1982). Indeed, some LC dendrites were found in the extra-TJ environment above SG2 (Fig. 5 B), where Birbeck granule formation was confirmed on the cell membrane of these penetrating dendrites (Fig. 5 C), further enforcing our confocal microscopy data. Fig. 5 A shows that diffusion of lanthanum nitrate is limited by TJs that seal SG2 cells. At the TJ penetration point, contact between LC and SG2 cells was also capable of stopping lanthanum diffusion, which was confirmed in serial ultrathin sections (Fig. 5 B, representative electron micrograph), indicating the presence of functional TJs between LC and SG2 cells.

Collectively, epidermal LCs elongate their dendrites through TJ barriers upon activation and engage in endocytic activity across TJ barriers. Taken-up Ags colocalized with langerin, strongly suggesting the involvement of Birbeck granule–associated mechanisms during this endocytic machinery (Fig. 5 D).